Title: The BMP antagonist *Gremlin1* contributes to the development of cortical excitatory neurons, motor balance and fear responses

Running Title: *Grem1* in cortical neuron development

Mari Ichinose[1,4)], Nobumi Suzuki[1,4)], Tongtong Wang[1,4)], Hiroki Kobayashi[1,2,4)], Laura Vrbanac[1,4)], Jia Q Ng[1,4)], Josephine A Wright[1,4)], Tamsin R M Lannagan[1,4)], Krystyna A Gieniec[1,4)], Martin Lewis[3,4)], Ryota Ando[2)], Atsushi Enomoto[2)], Simon Koblar[1,4)], Paul Thomas[1,4)], Daniel L Worthley[4)], Susan L Woods[1,4)]

1. School of Medicine, University of Adelaide, SA, Australia
2. Department of Pathology, Nagoya University Graduate School of Medicine, Nagoya, Japan
3. College of Medicine and Public Health, Flinders University, Bedford Park, SA, Australia
4. South Australian Health and Medical Research Institute, Adelaide, SA, Australia

Corresponding author: Susan L Woods
susan.woods@adelaide.edu.au

Key words

Grem1, BMP, cortical development, excitatory neuron

Summary statement

The BMP antagonist, *Grem1,* marks neuroprogenitors that give rise to deep layer glutamatergic neurons in the embryonic mouse brain. *Grem1* conditional knockout mice display cortical and behavioural abnormalities.

Abstract

Bone morphogenetic protein (BMP) signaling is required for early forebrain development and cortical formation. How the endogenous modulators of BMP signaling regulate the structural and functional maturation of the developing brain remains unclear. Here we show that expression of the BMP antagonist, *Grem1,* marks a neuroprogenitor that gives rise to layer Ⅴ and Ⅵ glutamatergic neurons in the embryonic mouse brain. Lineage tracing of *Grem1*-expressing cells in the embryonic brain was examined by administration of tamoxifen to pregnant *Grem1creERT; Rosa26LSLTdtomato* mice at 13.5 days post coitum (dpc), followed by collection of embryos later in gestation. In addition, at 14.5 dpc, bulk mRNA seq analysis of differentially expressed transcripts between FACS sorted *Grem1* positive and negative cells was performed. We also generated *Emx1-cre* mediated *Grem1* conditional knockout mice (*Emx1-Cre;Grem1*$^{flox/flox}$) in which the *Grem1* gene was deleted specifically in the dorsal telencephalon. *Grem1*^{Emx1cKO} animals had reduced cortical thickness, especially layers Ⅴ and Ⅵ and impaired motor balance and fear sensitivity compared to littermate controls. This study has revealed new roles for Grem1 in the structural and functional maturation of the developing cortex.

Introduction

48 During development of the nervous system, bone morphogenetic protein (BMP)
49 signaling has important roles in the promotion of dorsal identity, and the regulation
50 of cell proliferation and differentiation. Yet BMP function in the maturation of
51 neurons in vivo is poorly understood. Misregulation of BMP signaling has been
52 suggested to contribute to human neurodevelopmental conditions such as autism
53 spectrum disorders (Kumar et al., 2019), however a detailed understanding of the
54 exact role for BMP signaling in these disorders is lacking, in line with our imperfect
55 knowledge of the regulation of the BMP pathway in normal brain development.
56 The BMP ligands (BMP 2, 4, 5, 6 and 7) bind to type I (BmprIA, BmprIB, Acvr1)
57 and type II (BmprII, ActrIIA, and ActrIIB) receptors. BMP ligands are expressed
58 broadly in the telencephalon during early gestation in mice and then become more
59 tightly localized to the choroid plexus at 13.5 dpc (Furuta et al., 1997). BMPs have
60 also been derived from the mesenchyme of the brain, such as meninges and
61 endothelial cells (Imura et al., 2008, Choe and Pleasure, 2018). Both type I and II
62 BMP receptors are expressed in the telencephalon during development but this is
63 further restricted in adulthood to BmprII in the cortex and hippocampus and
64 ActrIIA/IIB in the dentate gyrus (Söderström et al., 1996). Aside from this
65 spatiotemporal regulation of receptors, the BMP signaling pathway is also regulated
66 by a family of secreted extracellular antagonists, that directly bind to the BMP
67 ligands to prevent interactions with BMP receptors both in development and disease
68 (Ali and Brazil, 2014). Antagonists such as Gremlin1 (Grem1), Noggin (Nog) and
69 Chordin (Chrd) have been shown to inhibit BMP action in a range of different cell
70 types and developmental stage-specific contexts to provide exquisite spatiotemporal
71 regulation of the pathway. The roles of Nog and Chrd have been partially elucidated:

72 they are required for forebrain development (Bachiller et al., 2000), as well as to
73 create a niche for adult hippocampal neurogenesis (Lim et al., 2000, Sun et al., 2007).
74 The expression and function of Grem1 in the developing brain has not yet been
75 determined. Grem1 is an extracellular secreted antagonist of BMP 2,4, and 7 that
76 signals to intestinal stem cells in the gut (Worthley et al., 2015) and plays a crucial
77 role in *Xenopus* dorsalisation (Hsu et al., 1998) and limb and kidney formation
78 (Khokha et al., 2003). Likewise the role of Grem1 in the normal adult CNS is
79 unmapped territory to date, outside of prior work in the pathogenic state of glioma
80 (Yan et al., 2014, Guan et al., 2017, Fu et al., 2018).

81 BMP signaling has been implicated in the regulation of forebrain patterning during
82 early embryogenesis, working together with other signaling pathways such as
83 fibroblast growth factor (FGF), Wnt, and Notch. High levels of BMP activity
84 suppresses anterior neural development, whereas abrogation of BMP signaling can
85 promote neural specification (Wilson and Houart, 2004, Lamb et al., 1993, Bachiller
86 et al., 2000). *In vitro* the addition of BMP 2 and 4 to mouse neural stem cell cultures
87 represses cell proliferation (Mathieu et al., 2008). BMP ligands regulate neuronal
88 differentiation as well as determination of glial cell fate, by promoting astrocyte
89 differentiation at the expense of oligodendrocytic fates (Mathieu et al., 2008, Yun et
90 al., 2004, Sun and Xu, 2010, Gomes et al., 2003).

91 Cortical neural stem cells (also known as radial glial cells, RGC) begin to divide
92 asymmetrically to start producing neurons at around 11.5 dpc in mice, signaling the
93 start of cortical development. RGC daughter cells detach from the ventricle and form
94 the first neuronal layer of the preplate by 13.5 dpc (Martynoga et al., 2012).
95 Subsequently born neurons migrate along RGCs and start to form the cortical plate,

96 separating the preplate into Cajal-Retzius cells in the marginal zone and subplate
97 neurons (Dwyer et al., 2016). The neocortex develops in an inside out manner, with
98 deep layers emerging first and superficial layers last. These neurons differentiate
99 into glutamatergic pyramidal neurons, whereas inhibitory interneurons are born in
100 the subcortical ganglionic eminences. Deep-layer pyramidal neurons (DLPNs, layer
101 V and VI) have both intratelenchephalic projections to superficial cortical layers and
102 extracephalic projections to other brain regions (Baker et al., 2018). Multiple
103 molecular mechanisms regulate this corticogenesis (Martynoga et al., 2012),
104 however the role of BMP signaling in cortical layer formation and functional
105 maturation of neurons has only been reported in limited studies so far. *In utero*
106 electroporation of BMP7 to murine 14.5 dpc cortical ventricular cells impaired
107 neuronal migration, suggesting BMP signaling regulates neuronal positioning and
108 migration (Choe and Pleasure, 2018). BMPs also regulate dendritogenesis and
109 neurite growth *in vitro* (Lee - Hoeflich et al., 2004, Matsuura et al., 2007). This is
110 consistent with a recent study that suggests perturbation of BMP signaling by
111 delivery of a dominant-negative version of BMP IB receptor affects migration,
112 polarity and dendritogenesis of mouse cortical neurons *in vivo* (Saxena et al., 2018).
113 To further establish the role of BMP signaling in forebrain development and
114 neuronal function, we focus here on the expression and function of the BMP
115 antagonist Grem1 in the developing mouse brain. We first assess *Grem1* expression
116 using transgenic *Grem1* reporter mice in the dorsal telencephalon and developing
117 neocortex. Next, to investigate the role of *Grem1* in the developing brain we use
118 transcriptomic analyses of sorted mouse *Grem1*-expressing cells and human single
119 cell RNA sequence (scRNAseq) data, combined with mouse neural stem/progenitor

120 cell (NSPC) culture *ex vivo*. Lastly, to examine the functional contribution of *Grem1*
121 to cortical development, we conditionally delete *Grem1* in the dorsal telecephalon
122 and undertake behavioural testing of mutant animals and littermate controls.
123

124 **Results**

125 ***Grem1* expressing cells are located in the dorsal telencephalon and give rise to deep**
126 **layer neocortical neurons**

127 To assess *Grem1* expression in the embryonic mouse brain we utilized transgenic
128 *Grem1creERT; Rosa26LSLTdtomato* reporter mice, in which tamoxifen treatment
129 results in expression of TdTomato in cells where the *Grem1* enhancer and promoter
130 sequences are active and the progeny of those cells (Worthley et al., 2015). Pregnant
131 *Grem1creERT; Rosa26LSLTdtomato* mice were administered tamoxifen at 11.5 dpc
132 and embryonic brains were collected 24 h later, but no TdTomato$^+$ cells were
133 observed, suggesting that *Grem1* is not yet expressed in the brain at this early time-
134 point (**Suppl Fig.1A**). Next, we administered tamoxifen to pregnant dams at 13.5 dpc,
135 and collected embryonic brains at 14.5, 17.5 and 20.5 dpc (**Fig.1A,B**). From this
136 timepoint we observed cells expressing TdTomato 24 hours after tamoxifen
137 administration located in the lower cortical plate and subplate of the dorsal
138 telencephalon, with dendrites extending to the pia matter (**Fig.1B,G**). ISH confirmed
139 that *Grem1* RNA was detected in almost all TdTomato$^+$ cells at 14.5 dpc, confirming
140 that the reporter line recapitulates endogenous *Grem1* expression. Six days later at
141 20.5 dpc, TdTomato$^+$ cell somas had migrated toward the lateral ventricle with
142 dendrites extending to the pia matter, becoming layer Ⅴ pyramidal neurons
143 (**Fig.1B,C**). Layer Ⅵ neurons were TdTomato$^+$ at 17.5 dpc and expanded in number

144 at 20.5 dpc (**Fig.1B,C**). ISH showed *Grem1* RNA was detected in most TdTomato$^+$
145 layer Ⅴ pyramidal neurons, but only 22% of layer Ⅵ neurons (**Fig.1C,D**). This
146 suggests that *Grem1* is actively expressed in layer V neurons but not layer Ⅵ
147 pyramidal neurons at 20.5 dpc. Cortical *Grem1* mRNA levels dramatically decrease
148 after birth as determined by qRT-PCR analysis of total RNA isolated from mouse
149 brain cortex at birth, p10 and 4w post-birth (**Fig.S1B**).
150 To confirm that *Grem1* + cells are actively dividing in order to give rise to their
151 traced progeny, we administered the thymidine analogue BrdU concomitantly with
152 tamoxifen to pregnant *Grem1creERT; Rosa26LSLTdtomato* dams at 13.5 dpc
153 (**Fig.1A**). BrdU is incorporated into newly synthesized DNA and so marks cells that
154 are dividing. 55% of TdTomato$^+$, layer Ⅴ pyramidal neurons cells are labelled with
155 BrdU at 17.5 dpc, demonstrating *Grem1* expressing cells at 13.5 dpc are progenitor
156 cells undergoing mitosis (**Fig.1E,F**). Fewer TdTomato$^+$ cells (17%) in layer Ⅵ were
157 BrdU positive, suggesting lower cell proliferation over the same period (**Fig.1F**). We
158 subsequently assessed whether TdTomato$^+$ cells express a marker of post-mitotic
159 mature neurons, NeuN, by immunohistochemistry. At 14.5 dpc most TdTomato$^+$ cells
160 were NeuN negative and were located in the subplate, and lower NeuN positive
161 cortical plate (**Fig.1G**). In contrast, later in gestation at 20.5 dpc almost all
162 TdTomato$^+$ cells in layer V and approximately half of those in layer VI express NeuN
163 (**Fig.1H**). This suggests that Grem1-lineage traced cells give rise to mature neurons
164 in the telencephalon.
165
166 **Global transcriptomic analysis defines transcript modules enriched in *Grem1*-**

167 **expressing cells**

168 To further characterise *Grem1* expressing cells in the developing mouse brain, we
169 undertook mRNAseq analysis on TdTomato$^+$ and negative cells from the
170 telencephalon. Pregnant *Grem1creERT; Rosa26LSLTdtomato* mice were
171 administered tamoxifen at 13.5 dpc and embryonic brains were collected at 14.5 dpc.
172 At this time-point almost all TdTomato$^+$ cells express endogenous *Grem1* RNA
173 (**Fig.1C**). Dissociated brain cells were flow sorted and live, TdTomato$^+$ and
174 TdTomato$^-$ cells were collected for transcriptomic analysis. TdTomato$^+$ cells
175 accounted for 5.1 ± 2.1% of all live cells (n=5) (**Fig.2A**). Bulk mRNA sequencing of
176 TdTomato$^+$ and TdTomato$^-$ populations and analysis of 1845 DEG between the two
177 cell populations revealed that *Grem1* was significantly upregulated in TdTomato$^+$
178 cells and BMP transcriptional target genes (Id1, Id3, Id4) were significantly
179 downregulated (adjusted P value (FDR) ≤ 0.05 (**Fig.2B**). We next undertook a
180 correlation analysis to identify modules of the 1845 DEGs that are coordinately
181 regulated in TdTomato$^+$ cells (**Fig.S2).** Shared membership of a module can suggest
182 genes that together perform a particular function. The clustering tree depicts the
183 topological distance between different modules, i.e. how similar or different the
184 expression of transcripts within the module are from other modules and highlighted
185 one module that contained 288 genes with particularly tightly correlated transcripts
186 (light green module, **Fig.S2).** Network visualization of the correlation analysis
187 showed that the majority of transcripts within this tightly correlated module are
188 upregulated in TdTomato$^+$ cells (magenta square, **Fig.2C)**. We investigated the
189 known function of genes within this module using a hypogeometric test for gene set
190 enrichment. Significantly enriched pathways (adjusted P value (FDR) ≤ 0.001) were

191 related to neuronal differentiation and projection, calcium signaling (possibly
192 associated with synapse functions) and axons (**Fig.2D**). The BMP target gene, *Id1*,
193 was identified as one of the central hub genes in this cluster and its expression was
194 significantly associated with other transcripts that have functions in neuronal
195 maturation (such as Lrrtm3, Ryr3) (**Fig.2E**). This suggests that neuronal functions
196 are upregulated in the *Grem1*-expressing TdTomato$^+$ cells of the developing
197 telencephalon, and that this biological function is linked, at least in part, to BMP
198 signaling.
199

200 ***Grem1/GREM1* is enriched in excitatory neuronal lineage cells during brain**
201 **development**

202 To further characterize the *Grem1*-expressing TdTomato$^+$ cell population we
203 undertook a candidate gene profiling approach using the bulk mRNAseq data. Gene
204 expression patterns of neuronal markers from a series of differentiation stages are
205 shown in **Fig.3A**. Immature neuronal markers, such as *Dcx, Ncam1, Neurod 2/6,*
206 *Tbr1*, were significantly upregulated at the RNA level in TdTomato$^+$ cells in
207 comparison to the TdTomato$^-$ cells at 14.5 dpc, while neural stem cell, radial glia,
208 and intermediate progenitor transcripts were significantly under-represented
209 ($p<0.05$). When RGCs (marked by co-expression of Sox2 and Pax6) generate
210 neocortical neurons, the expression of specific transcription factors can be used to
211 identify neurons within particular cortical layers(Martynoga et al., 2012). Our bulk
212 RNAseq analysis showed that transcripts encoding the layer Ⅴ marker, *Fezf2*, and
213 Ⅵ markers, *Tbr1* / *Sox5*, were significantly upregulated in *Grem1*-expressing

214 TdTomato$^+$ cells, whereas the RGC markers, *Sox2* and *Pax6* were significantly
215 downregulated (absolute value of log2 fold change≥2.0, FDR<0.05) and did not
216 colocalize with Tdtomato at 14.5 dpc by immunohistochemistry (**Fig.S3**).

217 To assist with identification of the neuronal subtype likely generated from *Grem1*-
218 expressing TdTomato$^+$ cells, we also performed GSEA on DEG transcripts between
219 TdTomato$^+$ and TdTomato$^-$ cells. We found a significant enrichment of a glutamate
220 secretion gene set in the DEGs (NES = 2.16 p = 0.0049) (**Fig.3B**), whereas GABAergic
221 and dopaminergic gene sets were not enriched (NES = -0.93 p = 0.75, NES = -0.69 p
222 = 0.87 respectively) (**Fig.S4A**). Consistent with the GSEA, glutamatergic neuron
223 markers, such as Slc17a7 (vGlut1), Grin1 and Grin2b were significantly upregulated
224 in Grem1 expressing cells at 14.5 dpc using a candidate gene approach, whereas
225 gabaergic and dopaminergic neuron markers, such as Slc6a1 (GABA transporter 1),
226 Gad1, Gad2, and Th (Tyrosine hydroxylase) were significantly downregulated
227 (p<0.05, **Fig.S4B**). Tbr1 plays a central role in the development of early-born cortical
228 excitatory neurons and regulates the connectivity of layer VI neurons (Hevner et al.,
229 2001). To confirm that Grem1 cells generate excitatory neuronal lineages, we
230 undertook immunohistochemical staining with Tbr1. This revealed *Grem1*-
231 expressing TdTomato$^+$ cells at 14.5 dpc expressed very low to no Tbr1, however they
232 did give rise to Tbr1$^+$ neurons in cortical layer VI at 20.5 dpc (**Fig.3C,D**).

233 To understand the relevance of our mouse focused study to the human setting, we
234 reanalyzed publicly available human scRNAseq data generated from human brain
235 at mid-gestation (22-23 weeks post-conception) (Fan et al., 2018). We categorized
236 each human cell in the dataset as either *GREM1*$^+$ or *GREM1*$^-$ based on the presence

237 or absence of *GREM1* RNAseq counts for each cell. Next, we compared the
238 transcriptional profiles of our mouse embryonic brain *Grem1*-expressing TdTomato$^+$
239 cells and TdTomato$^-$ cells, with the human mid-gestational brain *GREM1*$^+$ and
240 *GREM1*$^-$ cells using a multidimensional scaling plot (**Fig.S4C**). Samples within the
241 same group cluster tightly together, dimension 2 separates the samples along species
242 lines, while dimension 1 clearly shows a similar separation of samples based on
243 altered expression profiles depending on *Grem1/GREM1* status in mouse and human
244 developing brain (**Fig.S4C**). By mapping the *GREM1*$^+$ cells onto a tSNE plot
245 generated from the human scRNAseq data, this revealed that most *GREM1*-
246 expressing cells accumulated in the excitatory neuron cluster within the human mid-
247 gestational cortex (**Fig.3E**). Lastly, we analysed the expression of BMP-signaling
248 components in the human scRNAseq dataset (**Fig.S4D,S5**). Interestingly, of the
249 pathway antagonists and similar to *GREM1*, *Sclerostin domain-containing protein*
250 *1* (*SOSTDC1)* transcripts were also highly enriched in the excitatory neuron cluster,
251 with *CHRD*, *NOG*, *BMP Binding Endothelial Regulator* (*BMPER)* and *Follistatin*
252 (*FST)* transcripts also enriched in specific cell types (**Fig.S4D**). Transcripts encoding
253 BMP2,4,7 that are antagonized by GREM1 were detected in various cell populations,
254 however expression of *Bmp2,7* was inversely correlated with *Grem1* expression in
255 the excitatory neuron cell population suggesting paracrine pathway regulation
256 (**Fig.S5**). Expression of the BMP target genes, *Id1,3,4* was also inversely correlated
257 with *Grem1*-expression in excitatory neurons, consistent with our developmental
258 mouse brain data (Fig 2B). This highlights the complexity of regulation of BMP
259 signaling during development of the cortex.
260

261 **Grem1 promotes proliferation and neural differentiation in neural stem / progenitor**
262 **cells *ex vivo***

263 Next we collected NSPCs from embryonic brains of *Grem1*$^{flox/flox}$ mice at 14.5 dpc
264 and transduced the cells ex vivo with control, *Cre*-expressing or *Grem1*-expressing
265 lentivirus to generate control *Grem1*$^{flox/flox}$, *Grem1*$^{-/-}$ and *Grem1* over-expressing
266 (*Grem1*$^{O/E}$) primary cultures. Endogenous Grem1 was detected in *Grem1*$^{flox/flox}$
267 control cultures by western blot, with absent or elevated protein levels in *Grem1*$^{-/-}$
268 and *Grem1*$^{O/E}$ cultures, respectively (**Fig.4A**). Control *Grem1*$^{flox/flox}$ cultures were
269 responsive to BMP pathway induction as determined by increased BRE-luciferase
270 reporter activity and expression of the BMP target genes, *Id1/2/3/4*, following
271 addition of recombinant human BMP2 (**Fig.4B, Fig.S6A**). This induction of BRE-
272 reporter activity and increase in BMP target gene transcript levels was significantly
273 enhanced in *Grem1*$^{-/-}$ cells and attenuated in *Grem1*$^{O/E}$ cells (**Fig.4B, Fig.S6A**). This
274 confirmed that Grem1 acts as an antagonist of BMP2 and suppresses downstream
275 transcriptional targets in embryonic NSPCs.

276 We next employed neurosphere assays to determine the effect of Grem1 modulation
277 on proliferation of embryonic NSPCs. Only mitogen responsive cells proliferate to
278 form clusters termed neurospheres, where sphere size correlates with proliferative
279 ability (Mori et al., 2006, Reynolds and Rietze, 2005). *Grem1*$^{O/E}$ cells form
280 significantly more and larger neurospheres than control *Grem1*$^{flox/flox}$ cells, whereas
281 *Grem1*$^{-/-}$ cells form significantly fewer (**Fig.4D,E**). To understand this phenomenon
282 from the aspect of cell viability, we evaluated the proliferation rates of *Grem1*$^{flox/flox}$,
283 *Grem1*$^{-/-}$ and *Grem1*$^{O/E}$ cultures. Over-expression of *Grem1* significantly increased
284 the rate of NSPC proliferation compared to control *Grem1*$^{flox/flox}$ NSPCs, while

285 conversely the number of viable *Grem1*$^{-/-}$ cells did not increase over the 72h time
286 course analysed (**Fig.4F**). These results suggested that Grem1 contributes to the
287 proliferation of NSPCs. Following on from this observation, we wanted to assess the
288 role of Grem1 in the differentiation of NSPCs to neurons, astrocytes and
289 oligodendrocytes. When cultured in recombinant BMP2-containing differentiation
290 media, addition of 1ng/ml recombinant GREM1 significantly increased the number
291 of NSPCs that differentiated into Tuj1^{+} neurons and O4^{+} oligodendrocyte lineage
292 cells, and decreased the number of GFAP^{+} astrocytes, in comparison to vehicle
293 treated control NPSCs (**Fig.4G,H**). This suggests that Grem1 may regulate the
294 differentiation potential of NPSCs.
295
296 ***Grem1* is required for normal cortical development**
297 In order to assess the functional role of *Grem1* in mouse forebrain development in
298 vivo, we generated tissue-specific *Grem1* conditional knockout mice using the *empty*
299 *spiracles homeobox 1* (*Emx1*)-*cre* driver. We first verified that *Emx1-cre* generates
300 efficient cre-mediated recombination in the dorsal telencephalon at 14.5 dpc by
301 visualizing TdTomato^{+} cells in reporter *Emx1-cre ; Rosa26LSLTdtomato* mouse
302 brains (**Fig.S7A**). Next we confirmed that *Emx1-cre ; Grem1*$^{flox/flox}$ (*Grem1*
303 conditional knockout, *Grem1*^{cKO}) mice had a significant reduction in *Grem1* RNA in
304 the developing forebrain compared with cre negative littermate controls by ISH at
305 14.5 dpc (**Fig.5A**) and real time RT-PCR at postnatal day0 (**Fig.5B**). *Grem1*^{cKO} mice
306 were viable and fertile. To examine the morphological consequences of conditional
307 *Grem1* loss in the developing mouse brain we performed Nissl staining on tissue
308 samples from *Grem1*^{cKO} and cre negative littermate controls. At 10 weeks of age,

309 total cortical thickness was significantly reduced in *Grem1*^{cKO} mice in comparison
310 with *Grem1*$^{flox/flox}$ littermate controls both in males and females, due to significantly
311 thinner cortical layers Ⅴ and Ⅵ (**Fig.5C, Fig.S7B**). The position and thickness of
312 each layer was confirmed by immunohistochemistry using markers specific for each
313 layer, i.e. CDP for layer Ⅱ-Ⅳ, Ctip2 for layer Ⅴ and Ⅵ and Foxp2 for layer Ⅵ
314 (**Fig.5D,E**). Cellular density was also more sparse in *Grem1*^{cKO} mice in comparison
315 with *Grem1*$^{flox/flox}$ littermate controls (**Fig.S7C,D**). Conversely, the other predominant
316 region of *Emx1-cre* driver activity, the hippocampus, that has important functions
317 in memory for navigation pertinent to our behavioural testing, displayed normal
318 morphology and cell density in *Grem1*^{cKO} mice (**Fig.S7E**).
319 Our earlier transcriptional network analysis from bulk RNAseq data identified an
320 *Id1* associated gene cluster that was differentially regulated in the *Grem1*-
321 expressing TdTomato^{+} cells from the cortex at 14.5 dpc (**Fig.2E**). From this cluster,
322 *Lrrtm3* and *Ryr3* were selected for further analysis because of their known functions
323 in synapse development (Balschun et al., 1999, Um et al., 2016, Roppongi et al., 2017,
324 Futagi and Kitano, 2015, Linhoff et al., 2009). The expression of these two
325 transcripts were significantly downregulated in the cortex of *Grem1*^{cKO} mice
326 compared with littermate controls at postnatal day 10 (**Fig.S7F**). This provides
327 further evidence of the relationship between *Grem1* expression and these genes.
328

329 **Motor coordination and fear responses were impaired in *Grem1*^{cKO} mice**

330 To assess the functional consequences of embryonic *Grem1* deletion in the mouse
331 forebrain, we undertook behavioural testing with *Grem1*^{cKO} mice in comparison with

332 *Grem1*$^{flox/flox}$ littermate controls. We compared motor balance using the Rotarod test.
333 Latency to fall was significantly shorter in *Grem1*^{cKO} mice both for males and females,
334 suggesting an impaired motor balance with loss of *Grem1* (**Fig.5G**). During the open
335 field test used to assess exploratory behaviours, both male and female *Grem1*^{cKO}
336 mice spent significantly more time in the central area away from the walls than
337 littermate controls (**Fig.5G**). The total distance moved and velocity of movement were
338 similar between *Grem1*^{cKO} and littermate controls (data not shown). Behavioral
339 testing using an elevated plus maze also indicated that female *Grem1*^{cKO} mice spent
340 significantly more time in the open maze arms and entered into the open arms more
341 frequently than littermate controls (**Fig.5G**). Both of the exploratory behavior tests
342 indicate that conditional loss of *Grem1* leads to reduced anxiety-like behavior. Lastly,
343 we used the Y maze test, to assess the short-term memory of *Grem1*^{cKO} and
344 littermate controls. We observed no difference in the number of entries made to the
345 novel arm of the Y maze between groups (**Fig.S8**), suggesting that *Grem1* expression
346 is not required for short-term memory function.
347

348 **Discussion**

349 The spatiotemporal regulation of BMP signaling in brain development is poorly
350 understood. Here we focus on the expression and function of the BMP antagonist
351 Grem1 during brain development, using transgenic lineage tracing, gene expression,
352 in vitro culture and conditional knock out approaches.
353 In the developing mouse brain *Grem1* is first expressed at 13.5 dpc in the actively
354 dividing dorsal telencephalon cells that retain mitotic potential (**Fig.1E,F**). *Grem1*-
355 expression identifies neuroprogenitors committed to the NeuN+ layer Ⅴ and Tbr1+

356 VI neurons. Transcriptomic profiling using our mRNAseq data from embryonic
357 *Grem1*-reporter mouse brains and publicly available human developmental brain
358 scRNAseq data suggests that *Grem1/GREM1* expression is primarily associated with
359 markers of glutamatergic excitatory neuronal lineages, rather than GABAergic or
360 dopaminergic neurons or other cell types of the developing brain (**Fig.3B,E**,
361 **Fig.S4A,B**). Consistent with this, *Grem1* was not expressed in the ganglionic
362 eminences, from which GABAergic interneurons originate; nor were GABAergic
363 transcripts upregulated or enriched by GSEA in *Grem1*-expressing TdTomato$^+$ cells
364 in the dorsal telencephalon using bulk RNAseq analysis (**Fig.S4A, B**). Likewise
365 Grem1-lineage traced cortical neurons expressed the excitatory marker, Tbr1
366 (**Fig.3C**). *Grem1*-expression labels and generates important excitatory neuronal
367 lineages, i.e. pyramidal neurons, that play high-level cognitive functions in the
368 neocortex. As Grem1 expression is required for the correct development of early-born
369 excitatory neurons of the neocortex (**Fig.1G**), misregulation of BMP signaling likely
370 affects the balance between excitatory and inhibitory neuronal activities, which has
371 been implicated in neurodevelopmental disorders (Dani et al., 2005).
372 Our analysis of scRNAseq data from human midgestational cortex (22-23 weeks
373 post-conception) suggests that there is coordinated regulation of BMP agonists and
374 antagonists at this developmental stage in humans, but that there may be also be
375 functional redundancies (**Fig.S4D**). Noggin is the most extensively studied of the
376 BMP antagonists in the CNS, where it is a recognized neural inducer during
377 gastrulation (Lamb et al., 1993). Addition of recombinant Noggin to neural stem cells
378 promotes neuronal and suppresses astrocytic differentiation *in vitro* (Mikawa and
379 Sato, 2011). In our study, we confirmed that Grem1 acts as a BMP antagonist in

380 embryonic NSPC cultures, suppressing downstream BMP transcriptional targets
381 (**Fig.4,S6**). Similar to Noggin, we determined that Grem1 promotes proliferation and
382 neural differentiation, at the expense of astrocytic lineages *in vitro* (**Fig.4**). BMP
383 transcriptional targets were significantly downregulated in *Grem1*-expressing
384 TdTomato^{+} cells also in vivo (**Fig.2B**) and *Grem1*$^{+}$ excitatory neurons in the human
385 embryonic cortex (**Fig.S5**). Together these results suggest that Grem1 expressing
386 cells are fated to become neurons via antagonism of potential paracrine BMP signals
387 (**Fig.S4D,S5**) (Furuta et al., 1997, Imura et al., 2008, Choe and Pleasure, 2018).
388 Our histological analyses identified that the cortex (particularly neocortical layers
389 Ⅴ and Ⅵ) of *Grem1*^{cKO} animals is significantly thinner, with less cells, in
390 comparison to littermate controls, with no obvious morphological changes in the
391 hippocampus. Our in vitro experiments confirmed that Grem1 drives proliferation
392 and neuronal differentiation in NSPC, thus this cortical phenotype is likely due to
393 reduced proliferation of embryonic NSPCs in *Grem1*^{cKO} mice. Layer Ⅴ neurons
394 target the spinal cord, cerebellum, striatum and the thalamus (Shipp, 2007) and play
395 roles in movement preparation, movement guidance, and the execution of well-timed
396 movements (Baker et al., 2018, Li et al., 2015). The observed decrease in layer Ⅴ
397 neurons would lead to impaired preparation for and coordination of movement in
398 *Grem1*^{cKO} animals and explain the motor balance defect in these animals in
399 comparison to litter mate controls. Emerging evidence suggests that layer Ⅵ
400 neurons play a central role in modulating thalamic and cortical neurons during
401 sensory processing (Wang et al., 2016). Our behavioural testing confirmed that loss
402 of Grem1 expression significantly impaired fear sensitivity in *Grem1*^{cKO} animals,

403 compared to littermate controls, consistent with a deficiency in layer Ⅵ neurons
404 with roles in sensory connections. BMP signaling is known to promote
405 synaptogenesis (Xiao et al., 2013, Shen et al., 2004) and altered synaptogenesis can
406 affect both fear sensitivity and motor abilities (Ha et al., 2016, Wood and Shepherd,
407 2010). Network analysis of DEG between *Grem1*-expressing TdTomato^{+} and
408 TdTomato^{-} cells from the developing mouse dorsal telencephalon identified a gene
409 cluster of inter-related transcripts in which the BMP target gene, *Id1*, acts as a hub.
410 Genes in the cluster play roles in neuron morphogenesis, synapse and axon
411 maturation (**Fig.2D,E**). For example, *Leucine-rich-repeat transmembrane neuronal*
412 *proteins 3/4* (*Lrrtm3/4*) genes encode synapse organizing proteins critical for the
413 development and function of excitatory synapses (Um et al., 2016, Roppongi et al.,
414 2017, Linhoff et al., 2009). Likewise, the *Ryanodine receptor3* (*Ryr3*) gene encodes a
415 member of a family of receptors that shape synaptic transmissions(Balschun et al.,
416 1999) by amplifying spike-driven calcium signals in presynaptic terminals, and
417 consequently enhancing the efficacy of transmitter release (Futagi and Kitano, 2015).
418 In *Grem1*^{cKO} animals, the mRNA expression of *Lrrtm3* and *Ryr3* was significantly
419 decreased in comparison to littermate controls (**Fig.S7F**). These results suggest
420 *Grem1* may contribute to synapse formation and function by inhibiting BMP
421 signaling and expression of associated gene networks, the subject of further studies.
422 In summary, this is the first study to reveal the important function of Grem1 in
423 cortical development, particularly as a marker, and maker, of excitatory
424 neuroprogenitors. In the future, Grem1 may hold value beyond understanding the
425 cellular biology of brain development and function as we develop new approaches to
426 help tackle complex neurodevelopmental and neurological diseases.

427

428 **Materials and Methods**

429

430 **Mice**

431 *Grem1-CreERT* transgenic mice (Worthley et al., 2015) were crossed with *R26-*
432 *LSLTdTomato* mice (B6.Cg-*Gt(ROSA)26Sor*$^{tm14(CAG-tdTomato)Hze}$/J, JAX 007914) to
433 generate a tamoxifen-induced *Grem1* reporter line. Pregnant dams were
434 administered 6mg of tamoxifen by oral gavage to induce embryonic *Grem1*-tracing,
435 with some dams bearing 13.5 dpc embryos also intraperitoneally injected with 5-
436 Bromodeoxyuridine (BrdU, Roche, 40 mg/kg) to track cell division. *Grem1*$^{flox/flox}$
437 mice (Gazzerro et al., 2007) were crossed with *Emx1-cre* mice (B6.129S2-
438 *Emx1*$^{tm1(cre)Krj}$/J, JAX 005628) to generate *Emx1-cre* mediated *Grem1* conditional
439 knockout mice (*Emx1-cKO*). The line was maintained by crossing *Emx1*$^{-cre/+}$;
440 *Grem1* $^{flox/flox}$ mice with *Grem1*$^{flox/flox}$ mice.
441 All mice were on the C57BL6/J background and experimentation was conducted
442 following approval by SAHMRI Animal Ethics Committee (approval number
443 SAM284) in accordance with the Australian code for the care and use of animals for
444 scientific purposes, 8th edition.

445

446 **Preparation of single cell suspensions and flow cytometry**

447 Pregnant *Grem1creERT; Rosa26LSLTdtomato* mice were administered tamoxifen at
448 13.5 dpc. At 14.5 dpc, dorsal telencephalons of the embryos were dissected in cold
449 phosphate-buffered saline (PBS) and the meningeal membranes were removed.
450 Neurocult Enzymatic Dissociation kit (Stemcell Technologies) was used for cell

451 dissociation according to the manufacturer's protocol. Dissociated cells were
452 resuspended in FACS buffer containing DAPI (0.5μg/ml). Sorting and analyses were
453 carried out on a FACS Fusion flow cytometer (Becton-Dickinson). Dead cells were
454 excluded by gating on forward and side scatter and by eliminating DAPI-positive
455 events. The cells harvested from *cre* negative littermate control mice were used to
456 set background fluorescence levels. Viable cells were sorted into FACS buffer,
457 collected via centrifugation and resuspended in Trizol (Invitrogen) for RNA
458 extraction.
459
460 **RNA extraction and mRNA seq**
461 RNA was extracted from sorted cells in Trizol according to the manufacturer's
462 protocol with the exception of addition of glycogen (20μg/μl) and isopropanol
463 precipitation overnight at -80°C to maximize yield. RNA quality and quantity were
464 analyzed using a NanoDrop and TapeStation. Total RNA was converted to strand-
465 specific Illumina compatible sequencing libraries using the Nugen Universal Plus
466 mRNA-Seq library kit from Tecan (Mannedorf) as per the manufacturer's
467 instructions (MO1442 v2). Briefly, 500ng of total RNA was polyA selected and the
468 mRNA fragmented prior to reverse transcription and second strand cDNA synthesis
469 using dUTP. The resultant cDNA was end repaired before the ligation of Illumina-
470 compatible barcoded sequencing adapters. The cDNA libraries were strand selected
471 and PCR amplified for 12 cycles prior to assessment by Agilent Tapestation for
472 quality and Qubit fluorescence assay for quantity. Sequencing pools were generated
473 by mixing equimolar amounts of compatible sample libraries based on the Qubit
474 measurements. Sequencing of the library pool was performed with an Illumina

475 Nextseq 500 using single read 75bp (v2.0) sequencing chemistry.

476

477 **Bioinformatic analysis**

478 **RNAseq data processing**

479 Fastq files from the sequencing run were firstly subjected to quality controls with
480 FastQC version 0.11.3. Raw reads with low quality were removed using Trim Galore
481 alignment (Phred score less than 28 and/or reads contains adaptor sequences). After
482 trimming, all bases with low quality scores and adaptor sequences were removed.
483 The trimmed reads were mapped to Ensembl mouse genome (GRCm38) with STAR
484 2.4.2a. No more than 1 base mismatch was allowed. Only uniquely mapped reads
485 were retained. Option -quantMode was enabled to generate gene level quantification.
486 The counts files were then merged into an expression table for downstream
487 differential expression analysis.

488

489 **Differential expression analysis**

490 Differentially expressed genes (DEG) between the *Tdtomato*$^{+}$ (*Grem1* positive) and
491 *Tdtomato*$^{-}$ (*Grem1* negative) populations were analyzed with edgeR packages in R
492 version 3.6.0 (Robinson et al., 2010) . Reads were inspected through
493 multidimensional scaling plot and outliers were removed. TMM normalized counts
494 were log2-transformed and counts per million (CPM) obtained. Paired comparisons
495 between the *Tdtomato*$^{+}$ (*Grem1* positive) and *Tdtomato*$^{-}$ (*Grem1* negative)
496 populations were performed. DEG reported as significant were selected by requiring
497 both adjusted P value (FDR) ≤ 0.05 and absolute value of log2 fold change ≥ 2.0.

498

499 **Supervised Weighted Gene Correlation Network Analysis (WGCNA)**

500 Only DEGs were used for subsequent network analysis. The gene network was
501 constructed using the R package WGCNA following the procedure as described
502 (Langfelder and Horvath, 2008). After the low expression genes (FPKM < 1) had been
503 filtered out from all gene expression libraries, Pearson's correlation based adjacency
504 was calculated on the basis of pairwise correlations of gene expression within
505 *Tdtomato*$^{+}$ (*Grem1* positive) samples. Topological overlap of the correlations was
506 used to weight the edges of the correlation network. The higher the weight, the
507 stronger the interaction between two genes. Connectivity for a single gene was
508 calculated as the sum of weights relative to the rest of the genes, and the top 5% of
509 genes with the highest connectivity in the network defined as hub genes. For
510 visualisation, a heat map was generated using the TOMplot() function in WGCNA R
511 package (version 1.68), with dissimilarity topological overlap (1 - topological overlap),
512 employed for hierarchical clustering. To generate the network plot, the weights of
513 the network were cut off at 0.1. Hypergeometric enrichment tests for each module-
514 defined gene list were performed with the enricher() function, as part of
515 clusterProfiler R package version 3.13.0 (Yu et al., 2012). Bonferroni adjustment for
516 p value was used, only gene sets with an adjusted p value less than 0.05 were
517 considered for interpretation of the biological function modules.

518

519 **Gene set enrichment analysis (GSEA)**

520 To utilize the Molecular signatures database (MSigDB), we accessed all gene sets
521 (.gmt file, version 6.2) from the Broad Institute and chose a subset for further
522 analyses including BioCarta, Hallmark, Gene Ontology (GO), Kyoto Encyclopedia of

523 Genes and Genomes (KEGG), Pathway Interaction Database, and the Reactome
524 Pathway Database. To enable cross species comparisons, mouse gene ensembl IDs
525 were converted to human orthologous gene symbols using biomaRt R package,
526 version 2.41.7 (Durinck et al., 2009). Humanised gene lists for the whole
527 transcriptome were ranked based on logfc values by comparing TdTomato^{+} and
528 TdTomato^{-} cells. The R package clusterProfiler version 3.13.0 (Yu et al., 2012) was
529 used to scan through all the gene sets mentioned above, using Benjamini & Hochberg
530 adjusted p values.
531
532 **Analysis of publicly available single cell RNA seq dataset**
533 Single cell RNAseq raw expression data was accessed for human mid-gestational
534 brain (22 and 23 weeks post-conception) cortex samples from GSE103723 (Fan et al.,
535 2018). The cells from two individual samples were grouped together, with the sum
536 of reads calculated for each gene to represent the data structure of bulky
537 transcriptomics. The limma package(Ritchie et al., 2015) was used to remove batch
538 effects with removeBatchEffect() and to generate multidimensional scaling plots. To
539 understand the expression pattern of human *GREM1* and its possible contribution
540 to neural differentiation, normalized counts and tSNE coordinates were employed
541 for visualization using plots generated with ggplot2 package in R environment
542 (Wickham, 2009). To investigate cell types expressing BMP antagonists, pearson's
543 Chi-Square test of independence was performed in the R environment with
544 chisq.test() function. Testing variables were gene expression categorised into high
545 and low by median expression, and using cell type identifiers from the original
546 scRNAseq study (Fan et al., 2018). Scaled standardised residuals for each gene were

547 used to plot the heatmap with ComplexHeatmap package (Gu et al., 2016).

548

549 ***In situ* hybridization (ISH)**

550 All ISH analyses were performed on formalin-fixed and paraffin-embedded mouse
551 tissue samples using RNAscope technology (RNAscope 2.5 HD Detection Kit,
552 RNAscope Multiplex Fluorescent Reagent Kit v2, Advanced Cell Diagnostics)
553 following the manufacturer's instructions. Briefly, tissue sections were baked in a
554 dry oven (HybEZ II Hybridization System, Advanced Cell Diagnostics) at 60°C for 1
555 h and deparaffinized, followed by incubation with an H_2O_2 solution (Pretreat 1
556 buffer) for 10 min at RT. Slides were boiled in a target retrieval solution (Pretreat 2
557 buffer) for 15 min, followed by incubation with a protease solution (Pretreat 3 buffer)
558 for 30 min at 40°C. Slides were incubated with a mouse *Grem1* probe (NM_011824.4,
559 region 398-1359, catalogue number 314741) for 2 h at 40°C, followed by successive
560 incubations with signal amplification reagents. Staining was visualized with DAB
561 or TSA Plus Cyanine 5 (NEL745001KT, PerkinElmer;1:750). Combined ISH and
562 immunofluorescence (IF)/immunohistochemistry (IHC) was undertaken by first
563 performing ISH, followed by IF/IHC. For IF following ISH, the sections were blocked
564 with blocking buffer (X0909, Dako) and then incubated with a primary antibody
565 (rabbit polyclonal anti-RFP, Rockland, 600-401-379) overnight at 4℃. The sections
566 were washed in 1x T-PBS 3 times and then incubated with Alexa Fluor 555-
567 conjugated secondary antibody (Thermo Fisher Scientific) for 60 min at room
568 temperature. The sections were mounted with ProLong Gold antifade reagent
569 containing 4'6-diamidino-2-phenylindole (DAPI; Thermo Fisher Scientific), and
570 fluorescence was examined using an inverse immunofluorescence microscope BZ-

571 X710 (Keyence, Japan) with optical sectioning. For IHC following ISH, after
572 inactivation of endogenous alkaline phosphatase with alkaline phosphatase blocking
573 solution for 10 minutes (SP-6000, Vector Laboratories), the slides were blocked with
574 blocking buffer (X0909, Dako) and incubated with a primary antibody (rabbit
575 polyclonal anti-RFP, Rockland, 600-401-379) at 4 °C overnight. The sections were
576 washed with PBS three times, followed by incubation with a horse anti-rabbit IgG
577 polymer (MP-5401, Vector Laboratories) for 30 min at room temperature. The slides
578 were washed with TBS three times, and signal developed using an alkaline
579 phosphatase substrate (SK-5105, Vector Laboratories). The reaction was stopped by
580 washing in TBS four times, and slides were counterstained with hematoxylin,
581 dehydrated in EtOH, cleared in xylene, and coverslipped. Cells expressing more than
582 1 ISH signal were regarded as positive for Grem1 RNA.
583
584 **Real time RT-PCR**
585 RNeasy mini kits (Qiagen) were used to isolate RNA from snap frozen mouse brain
586 tissues. RNA was reverse-transcribed into cDNA with cDNA master (Sigma). PCR
587 amplification was performed with Kappa Sybr qPCR mix or Kappa Probe qPCR mix
588 using QuantStudio7 (Applied Biosystems). The mouse GAPDH gene was used as an
589 endogenous control. The following primers were used:
590 TaqMan probes and primers, Gremlin1 (IDT, Mm.PT.58.11631114), Id1
591 (IDT,Mm.PT.58.6622645.g), Id2 (IDT, Mm.PT.58.13116812.g), Id3 (IDT,
592 Mm.PT.58.29482466.g), Id4 (IDT, Mm.PT.58.6851535)
593 Sybr primers, Gapdh-forward AAGGTCATCCCAGAGCTGAA, Gapdh-reverse
594 CTGCTTCACCACCTTCTTGA Ryr3-forward TGCTGTCGCTTCCTTTGCTA, Ryr3-

595 reverse CATCGATGGGGACGCTAGAC, Lrrtm3-forward
596 TAGCAAATCAGGCTCCAGGG, Lrrtm3-reverse GAGTTCATGATGGACCCCACA
597
598 **Immunohistochemistry**
599 To collect 14.5 dpc, 17.5 dpc and 20.5 dpc embryonic brains, euthanized pregnant
600 dams immediately underwent cardiac perfusion with 4% PFA. Whole embryos at
601 14.5 dpc, or dissected embryonic brains for 17.5 and 20.5 dpc were fixed in 4% PFA
602 at 4℃ overnight. Embryos and brains were then cryoprotected in 30% sucrose and
603 frozen in OCT embedding medium. 16 μm sections were cut using a Leica CM1900
604 cryostat. To make paraffin sections, samples were post fixed in 10% neutral buffered
605 formalin overnight and processed. 5 μm sections were cut using a Leica HM325
606 microtome. Sections were blocked with Protein Block Serum-Free (Dako) for 1 hour
607 at room temperature, incubated overnight with first antibody at 4℃, secondary
608 antibody for 1 hour at room temperature, and coverslipped with Vectashield Antifade
609 Mounting Medium (Vector laboratories). The following antibodies were used: Anti-
610 TBR1(Abcam, ab183032, 1:400), Anti-NeuN (Abcam, ab104225, 1:500), Anti-β III
611 tubulin (Sigma, T5076, 1:400), Anti-O4 (R & D systems, MAB1326, 1:500), Anti-
612 GFAP (Dako, Z0334, 1:250), Anti-FOXP2 (Abcam, ab16046, 1:10000), Anti-Ctip2
613 (Abcam, ab18465, 1:800), Anti-CDP (Santa Cruz, sc-13024, 1:400), Anti-BrdU
614 (Abcam, ab6326, 1:600), Anti-RFP (Rockland, 600-401-379, 1:1000), Anti-Sox2
615 (Millipore, AB5603, 1:400), Anti-Pax6 (Millipore, AB2237, 1:100)
616 Images were acquired on a Leica SP5 spectral scanning confocal microscope.
617

618 **Neural stem cell and progenitor cell culture**

619 Before seeding cells, tissue culture dishes were coated with PDL (100μg/ml) and
620 laminin (10μg/ml). Embryonic neural stem and progenitor cells were isolated from
621 pregnant mice at 14.5 dpc. Dorsal telencephalons were dissected from each embryo
622 in PBS, meningeal membranes removed and the tissue triturated to a single cell
623 suspension. Cells were cultured in NeuroCult™ Proliferation Medium containing 20
624 ng/ml epidermal growth factor (EGF) (Stemcell Technologies). For differentiation
625 assays, cells were seeded onto 4 well chamber slides (Thermofisher #NUN177399) in
626 Neurocult Differentiation medium (Stemcell Technologies). To induce recombination
627 or overexpression of *Grem1*, cells collected from Grem1$^{flox/flox}$ embryos were infected
628 with plenti-EF1-*Cre-2a-sfGFP-2a-puro*, plenti-EF1-*Grem1-2a-sfGFP-2a-puro,* or
629 plenti-EF1-*2a-sfGFP-2a-puro* lentivirus, and transduced cells were selected using
630 puromycin for 5 days and used for experiments before passage 5. Lentivirus plasmids,
631 psPAX2 and MD2.G were transfected to 293T cells to generate lentivirus, and viral
632 supernatant was concentrated using Amicon-Ultra 100k spin columns. To assess
633 neurosphere forming ability, cells were seeded in 6-well uncoated plates ($1.6x10^5$
634 cells per well) and cultured for 5 days. The number of neurospheres sized 50-100 μm
635 and >100 μm was counted. For cell viability assays, neural stem / progenitor cells
636 were seeded in 96-well coated plates ($1x10^4$ cells per well) and RealTime-Glo™ MT
637 Cell Viability Assay (Promega) was used with the continuous-read protocol at 0, 24,
638 52 and 72 hours. Recombinant human BMP2 (Prospec) was added to the
639 differentiation medium.

640

641 **Luciferase assay**

642 BMP pathway activity was measured using the BMP response element luciferase
643 reporter pGL3 BRE luciferase (addgene #45126), internal control pRL/TK-luciferase
644 reporter and the dual luciferase reporter assay kit (Promega). Neural stem /
645 progenitor cells were seeded in coated 24-well plates ($1.6x10^5$ cells per well) and
646 transfected with the reporter plasmids using xTremeGENE HP DNA transfection
647 reagent (Roche). Cells were collected 48hr after transfection using Passive lysis
648 buffer (Promega). The pGL3 empty vector was used as a control for BMP-
649 independent changes in reporter activity.
650
651 **Western blot**
652 Cell lysates were solubilized with M-PER Mammalian Protein Extraction Reagent
653 containing complete protease and phosphatase inhibitors. Lysates were separated
654 by SDSPAGE and transferred to PVDF membranes (Millipore). After blocking with
655 5% nonfat skim milk in PBST for 30 min at room temperature, the membranes were
656 incubated overnight at 4℃ with anti-Gremlin1 antibody (R＆D systems, AF956,
657 1:1000) or anti-βActin (Santa Cruz, sc-47778, 1:1000) in 0.5% nonfat skim milk in
658 PBST. Membranes were washed with PBST and incubated with alkaline
659 phosphatase-conjugated secondary antibodies (anti-rabbit IgG and anti-mouse IgG,
660 GE healthcare life sciences, 1:10000) for 1 hr at room temperature. Finally, the blot
661 was visualized with Immobilon HRP substrate (Millipore) using a Chemi Doc XRS1
662 (Bio-Rad).
663
664 **Behavioral tests**
665 Mice were submitted to Rotarod, open field, elevated plus maze, and Y maze tests at

666 the age of 7-10 weeks. Mice while in their home cages were acclimatized to the
667 behavior suite for at least 30 min prior to testing. The data was acquired blindly to
668 the genotype.
669 Rotarod. Animals were placed on the rotarod (Panlab/Harvard Apparatus) that
670 linearly increased rotation speed from 4 to 40 rpm during a 120 second period. An
671 accelerating protocol was employed to eliminate the need for habituation to the
672 rotarod. This procedure was repeated for a total of three trials per mouse, separated
673 by 15min inter-trial intervals and the mean latency to fall from the rotarod in
674 seconds was compared between wild type littermate controls and *Grem1*^{cKO} mice to
675 assess motor coordination.
676 Open field test. The open field test was conducted in four identical square arenas
677 (50x50x50cm) surrounded by walls. Mice were individually placed in a corner of a
678 clean arena and allowed to explore for 10 min. For the purpose of data collection, the
679 arena was conceptually partitioned into two zones: a virtual center zone of 23x23 cm
680 and a peripheral zone occupying the remaining area. Lower percentages of time
681 spent in the center zone was used to indicate a higher level of anxiety.
682 Elevated plus maze test. The elevated plus maze consisted of a central square (8 × 8
683 cm) and four arms (29 cm long × 8 cm wide, two open arms with no railing and two
684 closed arms enclosed by a transverse wall 20 cm in height). A mouse was placed in
685 the center of the central square facing the open arm and allowed to explore the maze
686 apparatus for 10 min. The time spent in any of the open arms was recorded and used
687 as a measure of anxiety.
688 Y maze test. The apparatus consisted of three arms with an angle of 120° between
689 each of the two arms. Each arm was 40 cm long × 8 cm wide × 15 cm high. Visual

690 cues were placed on the walls of the mazes. The Y-maze test consisted of two trials
691 separated by an inter-trial interval (ITI) to assess spatial recognition memory. The
692 first trial (training) had a 5 min duration and allowed the mouse to explore only two
693 arms of the maze, with the third arm (novel arm) being blocked. After 30min ITI, the
694 second trial was conducted, during which all three arms were accessible for 5 min.
695 Trials were recorded using a ceiling-mounted camera and analyzed by a video
696 analyzer (Ethovision XT, Noldus) to determine the period that each mouse spent in
697 each arm of the maze.
698

699 **Statistics**

700 All statistical analyses were performed using Graphpad prism 8, with methods and
701 values summarised in each figure legend.
702

703 **Acknowledgements**

704 We thank Dr. Randall Grose (SAHMRI, Australia) for flow cytometry assistance; Dr
705 Mark van der Hoek and the Genomics Core (SAHMRI, Australia) for RNA-seq
706 library preparation and sequencing, Dr. Hiroaki Fujiwara (The Institute for Adult
707 Diseases, Asahi Life Foundation, Tokyo, Japan) for reviewing the manuscript;
708 Regeneron and Prof Andrew Zannettino for providing *Grem1*$^{flox/flox}$; *Emx1-cre* mice.
709

710 **Competing interests**

711 The authors declare no competing interests.
712

713 **Funding**

MI was supported by Japan Society for the Promotion of Science (JSPS) Overseas Research Fellowships and Overseas study grant of Kanzawa Medical Research Foundation; NS by fellowship grants from the Astellas Foundation for Research on Metabolic Disorders and the Uehara Memorial Foundation; DLW by a National Health & Medical Research Council (NHMRC) Career Development Fellowship; SLW by the Cancer Council SA Beat Cancer Project on behalf of its donors and the State Government of South Australia through the Department of Health (MCF0418 to SLW), HK by JSPS Overseas Challenge Program for Young Researchers, Takeda Science Foundation Fellowship and the Greaton International PhD Scholarship. This study was supported by grants from the NHMRC (APP1140236 to SLW, APP1099283 to DLW, APP1143414 to DLW/SLW), the KAKENHI Grant-in-Aid for Scientific Research (19K17478 to NS) and the Kanae Foundation Asia-Oceania Collaborative Research Grants to NS.

Data availability

The accession number for all sequencing data reported in this paper is GEO: GSEXXXXXX.

Reference

ALI, I. H. A. & BRAZIL, D. P. 2014. Bone morphogenetic proteins and their antagonists: current and emerging clinical uses. *British Journal of Pharmacology,* 171, 3620-3632.

BACHILLER, D., KLINGENSMITH, J., KEMP, C., BELO, J. A., ANDERSON, R. M., MAY, S. R., MCMAHON, J. A., MCMAHON, A. P., HARLAND, R. M., ROSSANT, J. & ROBERTIS, D. E. M. 2000. The organizer factors Chordin and Noggin are required for mouse forebrain development. *Nature,* 403, 658-661.

BAKER, A., KALMBACH, B., MORISHIMA, M., KIM, J., JUAVINETT, A., LI, N. & DEMBROW, N. 2018. Specialized Subpopulations of Deep-Layer Pyramidal Neurons in the Neocortex: Bridging Cellular Properties to Functional Consequences. *The Journal of neuroscience,* 38**,** 5441-5455.

BALSCHUN, D., WOLFER, D. P., BERTOCCHINI, F., BARONE, V., CONTI, A., ZUSCHRATTER, W., MISSIAEN, L., LIPP, H. P., FREY, U. J. & SORRENTINO, V. 1999. Deletion of the ryanodine receptor type 3 (RyR3) impairs forms of synaptic plasticity and spatial learning. *The EMBO Journal,* 18**,** 5264-5273.

CHOE, Y. & PLEASURE, S. J. 2018. Meningeal Bmps Regulate Cortical Layer Formation. *Brain Plasticity,* 4**,** 169-183.

DANI, V. S., CHANG, Q., MAFFEI, A., TURRIGIANO, G. G., JAENISCH, R. & NELSON, S. B. 2005. Reduced cortical activity due to a shift in the balance between excitation and inhibition in a mouse model of Rett syndrome. *Proceedings of the National Academy of Sciences of the United States of America,* 102**,** 12560-12565.

DURINCK, S., SPELLMAN, P. T., BIRNEY, E. & HUBER, W. 2009. Mapping identifiers for the integration of genomic datasets with the R/Bioconductor package biomaRt. *Nature Protocols,* 4**,** 1184-1191.

DWYER, N. D., CHEN, B., CHOU, S.-J., HIPPENMEYER, S., NGUYEN, L. & GHASHGHAEI, T. H. 2016. Neural Stem Cells to Cerebral Cortex: Emerging Mechanisms Regulating Progenitor Behavior and Productivity. *The Journal of Neuroscience,* 36**,** 11394-11401.

FAN, X., DONG, J., ZHONG, S., WEI, Y., WU, Q., YAN, L., YONG, J., SUN, L., WANG, X., ZHAO, Y., WANG, W., YAN, J., WANG, X., QIAO, J. & TANG, F. 2018. Spatial transcriptomic survey of human embryonic cerebral cortex by single-cell RNA-seq analysis. *Cell Research,* 28**,** 730-745.

FU, C., LI, D., ZHANG, X., LIU, N., CHI, G. & JIN, X. 2018. LncRNA PVT1 Facilitates Tumorigenesis and Progression of Glioma via Regulation of MiR-128-3p/GREM1 Axis and BMP Signaling Pathway. *Neurotherapeutics,* 15**,** 1139-1157.

FURUTA, Y., PISTON, D. W. & HOGAN, B. L. 1997. Bone morphogenetic proteins (BMPs) as regulators of dorsal forebrain development. *Development,* 124**,** 2203-2212.

FUTAGI, D. & KITANO, K. 2015. Ryanodine-receptor-driven intracellular calcium dynamics underlying spatial association of synaptic plasticity. *Journal of*

Computational Neuroscience, 39, 329-347.

GAZZERRO, E., SMERDEL-RAMOYA, A., ZANOTTI, S., STADMEYER, L., DURANT, D., ECONOMIDES, A. N. & CANALIS, E. 2007. Conditional Deletion of Gremlin Causes a Transient Increase in Bone Formation and Bone Mass. *Journal of Biological Chemistry,* 282, 31549-31557.

GOMES, W. A., MEHLER, M. F. & KESSLER, J. A. 2003. Transgenic overexpression of BMP4 increases astroglial and decreases oligodendroglial lineage commitment. *Developmental biology,* 255, 164-177.

GU, Z., EILS, R. & SCHLESNER, M. 2016. Complex heatmaps reveal patterns and correlations in multidimensional genomic data. *Bioinformatics,* 32, 2847-2849.

GUAN, Y., CHENG, W., ZOU, C., WANG, T. & CAO, Z. 2017. Gremlin1 promotes carcinogenesis of glioma in vitro. *Clinical and Experimental Pharmacology and Physiology,* 44, 244-256.

HA, S., LEE, D., CHO, Y., CHUNG, C., YOO, Y.-E., KIM, J., LEE, J., KIM, W., KIM, H., BAE, Y., TANAKA-YAMAMOTO, K. & KIM, E. 2016. Cerebellar Shank2 Regulates Excitatory Synapse Density, Motor Coordination, and Specific Repetitive and Anxiety-Like Behaviors. *Journal of Neuroscience,* 36, 12129-12143.

HEVNER, R. F., SHI, L., JUSTICE, N., HSUEH, Y.-P., SHENG, M., SMIGA, S., BULFONE, A., GOFFINET, A. M., CAMPAGNONI, A. T. & RUBENSTEIN, J. 2001. Tbr1 Regulates Differentiation of the Preplate and Layer 6. *Neuron,* 29, 353-366.

HSU, D. R., ECONOMIDES, A. N., WANG, X., EIMON, P. M. & HARLAND, R. M. 1998. The Xenopus dorsalizing factor Gremlin identifies a novel family of secreted proteins that antagonize BMP activities. *Molecular cell,* 1, 673-683.

IMURA, T., TANE, K., TOYODA, N. & FUSHIKI, S. 2008. Endothelial cell - derived bone morphogenetic proteins regulate glial differentiation of cortical progenitors. *European Journal of Neuroscience,* 27, 1596-1606.

KHOKHA, M. K., HSU, D., BRUNET, L. J., DIONNE, M. S. & HARLAND, R. M. 2003. Gremlin is the BMP antagonist required for maintenance of Shh and Fgf signals during limb patterning. *Nature genetics,* 34, 303-307.

KUMAR, S., REYNOLDS, K., JI, Y., GU, R., RAI, S. & ZHOU, C. J. 2019. Impaired neurodevelopmental pathways in autism spectrum disorder: a review of signaling mechanisms and crosstalk. *Journal of Neurodevelopmental*

Disorders, 11, 10.
LAMB, T. M., KNECHT, A. K., SMITH, W. C., STACHEL, S. E., ECONOMIDES, A. N., STAHL, N., YANCOPOLOUS, G. D. & HARLAND, R. M. 1993. Neural induction by the secreted polypeptide noggin. *Science (New York, N.Y.),* 262, 713-718.
LANGFELDER, P. & HORVATH, S. 2008. WGCNA: an R package for weighted correlation network analysis. *BMC Bioinformatics,* 9, 559.
LEE - HOEFLICH, S., CAUSING, C. G., PODKOWA, M., ZHAO, X., WRANA, J. L. & ATTISANO, L. 2004. Activation of LIMK1 by binding to the BMP receptor, BMPRII, regulates BMP - dependent dendritogenesis. *The EMBO Journal,* 23, 4792-4801.
LI, N., CHEN, T.-W., GUO, Z. V., GERFEN, C. R. & SVOBODA, K. 2015. A motor cortex circuit for motor planning and movement. *Nature,* 519, 51-56.
LIM, D. A., TRAMONTIN, A. D., TREVEJO, J. M., HERRERA, D. G., GARC A-VERDUGO, J. M. & ALVAREZ-BUYLLA, A. 2000. Noggin antagonizes BMP signaling to create a niche for adult neurogenesis. *Neuron,* 28, 713-726.
LINHOFF, M. W., LAUR N, J., CASSIDY, R. M., DOBIE, F. A., TAKAHASHI, H., NYGAARD, H. B., AIRAKSINEN, M. S., STRITTMATTER, S. M. & CRAIG, A. 2009. An Unbiased Expression Screen for Synaptogenic Proteins Identifies the LRRTM Protein Family as Synaptic Organizers. *Neuron,* 61, 734-749.
MARTYNOGA, B., DRECHSEL, D. & GUILLEMOT, F. 2012. Molecular Control of Neurogenesis: A View from the Mammalian Cerebral Cortex. *Cold Spring Harbor Perspectives in Biology,* 4.
MATHIEU, C., SII-FELICE, K., FOUCHET, P., ETIENNE, O., HATON, C., MABONDZO, A., BOUSSIN, F. D. & MOUTHON, M.-A. 2008. Endothelial cell-derived bone mo rphogenetic proteins control proliferation of neural stem/progenitor cells. *Molecular and Cellular Neuroscience,* 38, 569-577.
MATSUURA, I., ENDO, M., HATA, K., KUBO, T., YAMAGUCHI, A., SAEKI, N. & YAMASHITA, T. 2007. BMP inhibits neurite growth by a mechanism dependent on LIM-kinase. *Biochemical and Biophysical Research Communications,* 360, 868-873.
MIKAWA, S. & SATO, K. 2011. Noggin expression in the adult rat brain. *Neuroscience,* 184, 38-53.
MORI, H., NINOMIYA, K., KINO-OKA, M., SHOFUDA, T., ISLAM, M., YAMASAKI,

M., OKANO, H., TAYA, M. & KANEMURA, Y. 2006. Effect of neurosphere size on the growth rate of human neural stem/progenitor cells. *Journal of Neuroscience Research,* 84, 1682-1691.

REYNOLDS, B. A. & RIETZE, R. L. 2005. Neural stem cells and neurospheres—re-evaluating the relationship. *Nature Methods,* 2, 333-336.

RITCHIE, M. E., PHIPSON, B., WU, D., HU, Y., LAW, C. W., SHI, W. & SMYTH, G. K. 2015. limma powers differential expression analyses for RNA-sequencing and microarray studies. *Nucleic Acids Research,* 43.

ROBINSON, M. D., MCCARTHY, D. J. & SMYTH, G. K. 2010. edgeR: a Bioconductor package for differential expression analysis of digital gene expression data. *Bioinformatics,* 26, 139-140.

ROPPONGI, R. T., KARIMI, B. & SIDDIQUI, T. J. 2017. Role of LRRTMs in synapse development and plasticity. *Neuroscience Research,* 116, 18-28.

S DERSTR M, S., BENGTSSON, H. & EBENDAL, T. 1996. Expression of serine/threonine kinase receptors including the bone morphogenetic factor type II receptor in the developing and adult rat brain. *Cell and tissue research,* 286, 269-279.

SAXENA, M., AGNIHOTRI, N. & SEN, J. 2018. Perturbation of canonical and non-canonical BMP signaling affects migration, polarity and dendritogenesis of mouse cortical neurons. *Development,* 145.

SHEN, W., FINNEGAN, S., LEIN, P., SULLIVAN, S., SLAUGHTER, M. & HIGGINS, D. 2004. Bone morphogenetic proteins regulate ionotropic glutamate receptors in human retina. *European Journal of Neuroscience,* 20, 2031-2037.

SHIPP, S. 2007. Structure and function of the cerebral cortex. *Current Biology,* 17.

SUN, M., THOMAS, M. J., HERDER, R., BOFENKAMP, L. M., SELLECK, S. B. & O'CONNOR, M. B. 2007. Presynaptic Contributions of Chordin to Hippocampal Plasticity and Spatial Learning. *The Journal of Neuroscience,* 27, 7740-7750.

SUN, Y. & XU, Z. 2010. Regulation of neural stem cell by bone morphogenetic protein (BMP) signaling during brain development. *Frontiers in Biology,* 5, 380-385.

UM, J., CHOI, T.-Y., KANG, H., CHO, Y., CHOII, G., UVAROV, P., PARK, D., JEONG, D., JEON, S., LEE, D., KIM, H., LEE, S.-H., BAE, Y.-C., CHOI, S.-Y., AIRAKSINEN, M. S. & KO, J. 2016. LRRTM3 Regulates Excitatory Synapse Development through Alternative Splicing and Neurexin Binding. *Cell Reports,* 14, 808-822.

WANG, W., ANDOLINA, I. M., LU, Y., JONES, H. E. & SILLITO, A. M. 2016. Focal

Gain Control of Thalamic Visual Receptive Fields by Layer 6 Corticothalamic Feedback. *Cerebral Cortex*.

WICKHAM, H. 2009. *Ggplot2 : elegant graphics for data analysis,* New York, Springer.

WILSON, S. W. & HOUART, C. 2004. Early Steps in the Development of the Forebrain. *Developmental Cell,* 6, 167-181.

WOOD, L. & SHEPHERD, G. 2010. Synaptic circuit abnormalities of motor-frontal layer 2/3 pyramidal neurons in a mutant mouse model of Rett syndrome. *Neurobiology of Disease,* 38, 281-287.

WORTHLEY, D. L., CHURCHILL, M., COMPTON, J. T., TAILOR, Y., RAO, M., SI, Y., LEVIN, D., SCHWARTZ, M. G., UYGUR, A., HAYAKAWA, Y., GROSS, S., RENZ, B. W., SETLIK, W., MARTINEZ, A. N., CHEN, X., NIZAMI, S., LEE, H., KANG, P. H., CALDWELL, J.-M., ASFAHA, S., WESTPHALEN, B. C., GRAHAM, T., JIN, G., NAGAR, K., WANG, H., KHEIRBEK, M. A., KOLHE, A., CARPENTER, J., GLAIRE, M., NAIR, A., RENDERS, S., MANIERI, N., MUTHUPALANI, S., FOX, J. G., REICHERT, M., GIRAUD, A. S., SCHWABE, R. F., PRADERE, J.-P., WALTON, K., PRAKASH, A., GUMUCIO, D., RUSTGI, A. K., STAPPENBECK, T. S., FRIEDMAN, R. A., GERSHON, M. D., SIMS, P., GRIKSCHEIT, T., LEE, F. Y., KARSENTY, G., MUKHERJEE, S. & WANG, T. C. 2015. Gremlin 1 Identifies a Skeletal Stem Cell with Bone, Cartilage, and Reticular Stromal Potential. *Cell,* 160, 269-284.

XIAO, L., MICHALSKI, N., KRONANDER, E., GJONI, E., GENOUD, C., KNOTT, G. & SCHNEGGENBURGER, R. 2013. BMP signaling specifies the development of a large and fast CNS synapse. *Nature Neuroscience,* 16, 856-864.

YAN, K., WU, Q., YAN, D. H., LEE, C. H., RAHIM, N., TRITSCHLER, I., DEVECCHIO, J., KALADY, M. F., HJELMELAND, A. B. & RICH, J. N. 2014. Glioma cancer stem cells secrete Gremlin1 to promote their maintenance within the tumor hierarchy. *Genes & Development,* 28, 1085-1100.

YU, G., WANG, L.-G., HAN, Y. & HE, Q.-Y. 2012. clusterProfiler: an R Package for Comparing Biological Themes Among Gene Clusters. *OMICS: A Journal of Integrative Biology,* 16, 284-287.

YUN, K., MANTANI, A., GAREL, S., RUBENSTEIN, J. & ISRAEL, M. A. 2004. Id4 regulates neural progenitor proliferation and differentiation in vivo. *Development,* 131, 5441-5448.

918 **Figure legends**

919 **Fig.1 *Grem1*-expressing cells give rise to cortical neurons in the developing mouse**

920 **brain**

921 (A) Schematic showing tamoxifen and BrdU administration to *Grem1creERT;*

922 *Rosa26LSLTdtomato* (*Grem1*-reporter) mice.

923 (B) Representative images of TdTomato$^+$ (red) cells in the telencephalon at 14.5dpc

924 (24h post-induction), 17.5dpc (3d post-induction), and 20.5dpc (6d post-induction)

925 in *Grem1*-reporter mice treated with tamoxifen at 13.5 dpc, DAPI (blue). Scale bar

926 = 200 μm.

927 (C) Representative images of immunohistochemical staining of boxed region from

928 (B) to visualize TdTomato$^+$ cells (red) and *Grem1* mRNA by ISH (green) at 14.5dpc

929 (I, 24h post-induction) and 20.5dpc (III, 6d post-induction) in *Grem1*-reporter mice

930 treated with tamoxifen at 13.5 dpc, DAPI (blue). The boxed areas were further

931 magnified in adjacent panels. Scale bar = 50 μm.

932 (D) Quantification of (C) showing the percentage of TdTomato$^+$ cells that were also

933 *Grem1* RNA$^+$ in 4 HPFs of 2-3 biological replicates, t-test.

934 (E) Representative images of immunofluorescence staining of (II) 17.5dpc

935 telencephalon from *Grem1*-reporter (red) mice induced with tamoxifen at dpc13.5,

936 BrdU (green), DAPI (blue). Scale bar = 50 μm.

937 (F) Quantification of (E) showing the percentage of TdTomato$^+$ cells that were also

938 BrdU$^+$ 2 HPFs of 3 biological replicates, t-test.

939 (G) Representative images of immunofluorescence staining of 14.5 and 20.5 dpc

940 neocortex from *Grem1*-reporter (red) mice induced with tamoxifen at dpc13.5, NeuN

941 (green), DAPI (blue). Layer V and VI boxed in (ⅰ) and (ⅱ), respectively. Scale bar =

942 50 μm. MZ, marginal zone ; CP, cortical plate ; SP, subplate

943 (H) Quantification of (G) showing the percentage of TdTomato$^+$ cells that were also

944 NeuN$^+$ in 3 HPF from 3 biological replicates. One way ANOVA with Tukey's multiple

945 test.

946 *p<0.05, **p<0.01, ***p<0.001, ****p<0.0001

947

948 **Fig.2 Grem1 expressing cells have neuron associated gene signatures**

949 (A) TdTomato$^+$ and TdTomato$^-$ cells were isolated from 14.5 dpc brains of *Grem1-*

950 *CreERT; R26-TdTomato* mice induced with tamoxifen at 13.5dpc. Representative

951 FACS plot is shown, n=5 mice sorted for bulk RNAseq analysis.

952 (B) Volcano plot to show differentially expressed genes (DEG) between

953 TdTomato$^+$.and TdTomato$^-$ cells from (A). *Grem1* was significantly upregulated,

954 whereas BMP target genes, *Id1,3,4* were significantly downregulated in TdTomato$^+$

955 cells compared to TdTomato$^-$ cells . Absolute value of log2 fold change ≥ 2.0,

956 FDR<0.05

957 (C) Network visualization of correlated DEG modules in TdTomato$^+$ cells. Each dot

958 represents a gene, dot perimeter colour indicates module membership (see Fig S3),

959 dot interior colour denotes upregulation (red) or downregulation (blue) of gene

960 transcript in TdTomato$^+$ cells compared to TdTomato$^-$, dot size indicates the

961 magnitude of gene expression correlation to neighboring genes, lines connecting dots

962 represent topological distance. The module containing highly correlated genes that

963 were predominantly upregulated in TdTomato$^+$ cells is boxed in magenta.

964 (D) Significantly enriched gene sets in magenta boxed module in (C). FDR<0.001

965 (E) Genes associated with Id1, a hub gene in the magenta boxed module in (C). Dot

966 perimeter colour indicates module membership (see Fig S3), dot interior colour
967 denotes upregulation (red) or downregulation (blue) of gene transcript in TdTomato^{+}
968 cells compared to TdTomato^{-}.
969
970 **Fig.3 *Grem1* is expressed in the glutamatergic excitatory neuron lineage cells**
971 (A) Heatmap depicting unsupervised clustering of TdTomato^{+} and TdTomato^{-} cells
972 isolated from 14.5dpc *Grem1*-reporter (red) mice induced with tamoxifen at dpc13.5
973 based on expression of representative differentiation marker transcripts for neural
974 stem cell (NSC), radial glia, intermediate progenitor, immature neuron, and mature
975 neuron.
976 (B) Gene set enrichment analysis (GSEA) for Glutamate Secretion genes between
977 TdTomato+ and TdTomato^{-} samples from (A). Normalised enrichment score (NES)
978 = 2.16, p = 0.0049.
979 (C) Representative images of immunofluorescence staining of 14.5 and 20.5 dpc
980 telencephalon from *Grem1*-reporter (red) mice induced with tamoxifen at dpc13.5,
981 TBR1 (green), DAPI (blue). Scale bar = 100 μm.
982 (D) Quantification of (C) showing the percentage of TdTomato^{+} cells that were also
983 TBR1^{+} in 3 representative fields from 3 biological replicates.
984 (E) tSNE plot of human scRNAseq dataset. *GREM1* expressing cells outlined in black.
985 Dot size represents Grem1 expression value as indicated.
986
987 **Fig.4 Gremlin1, a BMP antagonist, promotes proliferation and neuronal**
988 **differentiation in neural stem / progenitor cells *ex vivo***
989 (A) Detection of Grem1 protein levels in control *Grem1*$^{flox/flox}$, *Grem1*$^{-/-}$ and *Grem1*$^{O/E}$

990 NSPC by western blot.

991 (B) BRE-reporter activity relative to internal control reporter. Data obtained from 4

992 independent experiments each performed in triplicate.

993 (C) BMP target gene, *Id1*, mRNA expression normalized to *Gapdh* in *Grem1*$^{flox/flox}$,

994 *Grem1*$^{-/-}$ and *Grem1*$^{O/E}$ NSPC treated with vehicle or rBMP2 for 24h. Columns, mean;

995 bars, SD. One way ANOVA with Tukey's multiple test. Results from 5 independent

996 experiments performed in triplicate.

997 (D) Representative images of *Grem1*$^{flox/flox}$, *Grem1*$^{-/-}$ and *Grem1*$^{O/E}$ neurosphere

998 cultures. Scale bar = 100 μm.

999 (E) Quantification of neurosphere number and size from (D) in 4 representative fields

1000 from 4 independent experiments. One way ANOVA with Tukey's multiple test.

1001 (F) Cell viability normalized to 0h timepoint for each culture. Results from 3

1002 independent experiments each performed in triplicate and analyzed using linear

1003 regression.

1004 (G) Representative images of immunofluorescence staining to identify Tuj1^{+} neurons,

1005 GFAP^{+} astrocytes and O4^{+} oligodendrocytes in differentiated cultures from wild type

1006 NSPCs treated with vehicle or rGrem1.

1007 (H) Quantification of (G), showing the percentage of marker^{+} cells in 3 representative

1008 fields from 3 independent experiments. t-test. Scale bar = 100 μm.

1009 *p<0.05, **p<0.01, ***p<0.001, ****p<0.0001

1010

1011 **Fig.5 Cortical development, motor balance, and fear is impaired in Grem1**

1012 **conditional knock out mice**

1013 ***Grem1* is required for normal cortical development**

1014 (A) Representative *Grem1* expression in the dorsal telencephalon of *Grem1*^{cKO} mice
1015 and *Grem1*$^{flox/flox}$ littermate controls by ISH at 14.5 dpc. Monochrome images were
1016 prepared for quantitation of the *Grem1* ISH signal with ImageJ. n = 3
1017 (B) *Grem1* mRNA levels normalized to *Gapdh* were determined using real time
1018 qRT-PCR in mouse cortical brain samples collected at postnatal day 0 from *Grem1*^{cKO}
1019 mice and littermate controls n=4 biological replicates. Columns, mean; bars, SD. t-
1020 test. ****p<0.0001
1021 (C) Representative histological images of cortical layers of *Grem1*^{cKO} mice and
1022 *Grem1*$^{flox/flox}$ littermate controls using Nissl at 10 weeks of age. Scale bar = 100 μm.
1023 (D) Quantification of cortical layer thickness from (C) compared in 8 pairs of male
1024 *Grem1*^{cKO} mice and littermate controls at 10 weeks of age. Female, n=7 control and
1025 n=7 *Grem1*^{cKO} . t-test, *p<0.05.
1026 (E) Representative images of immunofluorescence staining of cortex of *Grem1*^{cKO}
1027 mice and littermate controls at 10 weeks of age to visualise layer Ⅱ-Ⅳ with
1028 marker CDP (green), layer Ⅴ and Ⅵ with marker Ctip2 (red), and DAPI (blue). n =
1029 3 Scale bar = 100 μm.
1030 (F) Representative images of immunohistochemical staining of cortex of *Grem1*^{cKO}
1031 mice and littermate controls at 10 weeks of age to visualise layer Ⅵ marker Foxp2
1032 IHC (shown in red arrowheads). n = 3 Scale bar = 100 μm.
1033 (G) Behavioral testing was performed to compare *Grem1*^{cKO} and *Grem1*$^{flox/flox}$ mice
1034 using age and sex matched littermates at 7-10 weeks of age. Columns, mean; bars,
1035 SEM.
1036 (i) Rotarod test latency to fall. Male, n=14 control and n=11 *Grem1*^{cKO} , Female, n=12

1037 control and n=13 *Grem1*^{cKO}. t-test, *p<0.05.

1038 (ii) Open field test, cumulative duration spent in the center area. Male, n=13 control

1039 and n=14 *Grem1*^{cKO}, Female, n=13 control and n=13 *Grem1*^{cKO}. t-test, *p<0.05.

1040 (iii, iv) Elevated plus maze test. (iii) Cumulative duration spent in open arms. (iv)

1041 The number of entries to open arms. Male, n=12 control and n=11 *Grem1*^{cKO}, Female,

1042 n=14 control and n=14 *Grem1*^{cKO}. t-test, *p<0.05.

1043

1044 **Fig.S1 *Grem1* starts to express after 12.5 dpc and is dramatically decreased after**

1045 **birth**

1046 (A) Representative coronal images of immunofluorescence staining of 12.5 dpc

1047 telencephalon from *Grem1*-reporter (red) mice induced with tamoxifen at 11.5 dpc.

1048 Scale bar = 100 μm. LV, lateral ventricle ; NCx, neocortex

1049 (B) *Grem1* mRNA levels normalized to *Gapdh* were determined using real time qRT-

1050 PCR in mouse cortical brain samples collected at p0, p10 and 4 weeks post-birth

1051 (n=4-6 mice/group, PCR conducted in triplicate) Columns, mean; bars, SD. One way

1052 ANOVA with Tukey's multiple test. ****p<0.0001

1053

1054 **Fig.S2 Clustering of differentially expressed genes**

1055 A heat map was generated to visualise the unsupervised hierarchical clustering of

1056 correlation scores for gene expression of DEG in TdTomato^{+} cells. Yellow colour

1057 indicates closely related and red not related. The color bar between the hierarchical

1058 clustering tree and plotting fields denotes the module membership of each gene.

1059

1060 **Fig.S3 *Grem1*-expressing cells are radial glial stem cell markers, Sox2 and Pax6**
1061 **negative**
1062 Representative images of immunofluorescence staining of 14.5 dpc neocortex from
1063 *Grem1*-reporter (red) mice induced with tamoxifen at dpc13.5, (A) Sox2 (green),
1064 DAPI (blue). (B) Pax6 (green), DAPI (blue). Scale bar = 100 μm.
1065
1066 **Fig.S4 Extended transcriptome analysis of bulk mRNAseq data from *Grem1*-**
1067 **expressing TdTomato$^+$ and TdTomato$^-$ telencephalon cells at 14.5dpc**
1068 (A) Gene set enrichment analysis (GSEA) for genes involved in the regulation of (i)
1069 GABAergic synaptic transmissions and (ii) dopamine secretion that were
1070 differentially regulated between *Grem1*-expressing TdTomato$^+$ and TdTomato$^-$
1071 cells. Normalised enrichment score (NES) = -0.93, p = 0.75 and NES = -0.69, p =
1072 0.87.
1073 (B) Unsupervised clustering of *Grem1*-expressing TdTomato$^+$ and TdTomato samples
1074 based on expression of representative markers for glutamatergic, GABAergic, and
1075 Dopaminergic neurons, in bulk mRNAseq data. Marker transcript expression is
1076 displayed as a heat map with high expression in red to low expression in blue.
1077 (C) Multidimensional scaling plot comparison of transcriptome of TdTomato$^+$ and
1078 TdTomato$^-$ cells isolated from 14.5dpc *Grem1*-reporter mice induced with tamoxifen
1079 at dpc13.5 and *GREM1$^+$* and *GREM1$^-$* cells from scRNAseq of human mid-gestational
1080 cortex.
1081 (D) GREM1 expression is associated with the excitatory neuronal lineage in the
1082 developing human cortex. Unsupervised clustering of human developmental brain
1083 cell populations from scRNAseq GSE103723 based on expression of lineage markers

1084 and transcripts encoding BMP antagonists (*FST, NOG, CHRD, BMPER, GREM1,*
1085 *SOSTDC1*), and BMP target genes *(ID1-4)*. Cell type is indicated by colour legend as
1086 per tSNE plot shown in Figure 4E. Chi-square testing was used to evaluate the level
1087 of each transcript in each cell population and the resulting standardized residual
1088 values are depicted in the heat map.
1089
1090 **Fig.S5 Grem1 suppresses intrinsic BMP signaling in developing human excitatory**
1091 **neurons, likely via antagonism of paracrine BMP ligands.**
1092 (A) Heat map depicting expression of BMP ligands in human developmental brain
1093 cell populations from scRNAseq GSE103723. Cell types as per tSNE plot shown in
1094 Figure 4E. Chi-square testing was used to evaluate the level of each transcript in
1095 each cell population and the resulting standardized residual values are depicted in
1096 the heat map.
1097 (B) GREM1 expression inversely correlates with enrichment of BMP2,7 and BMP
1098 target genes ID1, 3, 4 expression in human excitatory neurons in mid-gestation.
1099 Expression of transcripts encoding BMP ligands antagonised by GREM1 and ID
1100 target genes in *GREM1*$^{+}$ and *GREM1*$^{-}$ cells is displayed from human scRNAseq
1101 GSE103723. One way ANOVA with Tukey's multiple test. ns $p>0.05$, *$p<0.05$,
1102 **$p<0.01$,****$p<0.0001$
1103
1104 **Fig.S6 Grem1 acts to antagonize BMP signaling in NSPCs resulting in altered**
1105 **downstream transcript levels**
1106 Transcript levels of BMP target genes, *Id2*, *Id3* and *Id4,* normalized to *Gapdh* in
1107 *Grem1*$^{flox/flox}$, *Grem1*$^{-/-}$ and *Grem1*$^{O/E}$ NSPC treated with vehicle or rBMP2 for 24h.

1108 Results from 5 independent experiments performed in triplicate. Columns, mean;
1109 bars, SD. One way ANOVA with Tukey's multiple test. *p<0.05, ***p<0.001
1110
1111 **Fig.S7 Extended morphological, immunostaining and transcript analysis of**
1112 ***Grem1*^{cKO} mice and littermate controls**
1113 (A) Representative coronal section of TdTomato^{+} (red) cells in the dorsal
1114 telencephalon at 14.5dpc in *Emx1-cre ; Rosa26LSLTdtomato* mouse brain. This cre-
1115 driver is broadly active across the telencephalon region in which *Grem1* is highly
1116 expressed. Scale bar = 100 μm. NCx, neocortex ; H, hippocampus ; Str, striatum ; T,
1117 thalamus
1118 (B) Quantification of cortical layer thickness compared between age and sex matched
1119 littermates at 10 weeks of age. Female, n=7 control and n=7 *Grem1*^{cKO},. t-test,
1120 *p<0.05.
1121 (C) Representative histological images of neocortical layer 5 and 6 from *Grem1*^{cKO}
1122 mice and *Grem1*$^{flox/flox}$ littermate controls at 10 weeks of age using Nissl. Scale bar =
1123 20um.
1124 (D) Quantification of (C) showing the cell number per area of layer V and Ⅵ using
1125 Nissl in 2 HPF of 3 biological replicates. Columns, mean; bars, SD. t-test. *p<0.05.
1126 Scale bar = 20um.
1127 (E) Representative histological images of hippocampus from *Grem1*^{cKO} mice and
1128 *Grem1*$^{flox/flox}$ littermate controls at 10 weeks of age using Nissl. 8 pairs of males and
1129 7 pairs of females were analyzed. Scale bar = 200 μm.
1130 (F) Transcripts from the *Id1* associated gene cluster (Fig3E), *Ryr3* and *Lrrtm3* were
1131 evaluated in *Grem1*^{cKO} and *Grem1*$^{flox/flox}$ littermate control cortex at p10 using real

1132 time qRT-PCR. *Ryr3* and *Lrrtm3* levels were normalized to *Gapdh*. n=4-6 biological
1133 replicates. Columns, mean; bars, SD. t-test. *p<0.05, ****p<0.0001
1134
1135 **Fig.S8 Memory is not impaired in *Grem1*^{cKO} mice compared to *Grem1*$^{flox/flox}$**
1136 **littermate controls**
1137 (A,B) Y maze test. Behavior was compared between age and sex matched *Grem1*^{cKO}
1138 mice and *Grem1*$^{flox/flox}$ littermate controls at 7-10 weeks of age. Male, n=12 control
1139 and n=10 *Grem1*^{cKO}, Female, n=14 control and n=13 *Grem1*^{cKO}. t-test. (A)
1140 Cumulative duration spent in new arm of Y maze. (B) The number of entries to new
1141 arm of the Y maze. Columns, mean; bars, SEM.

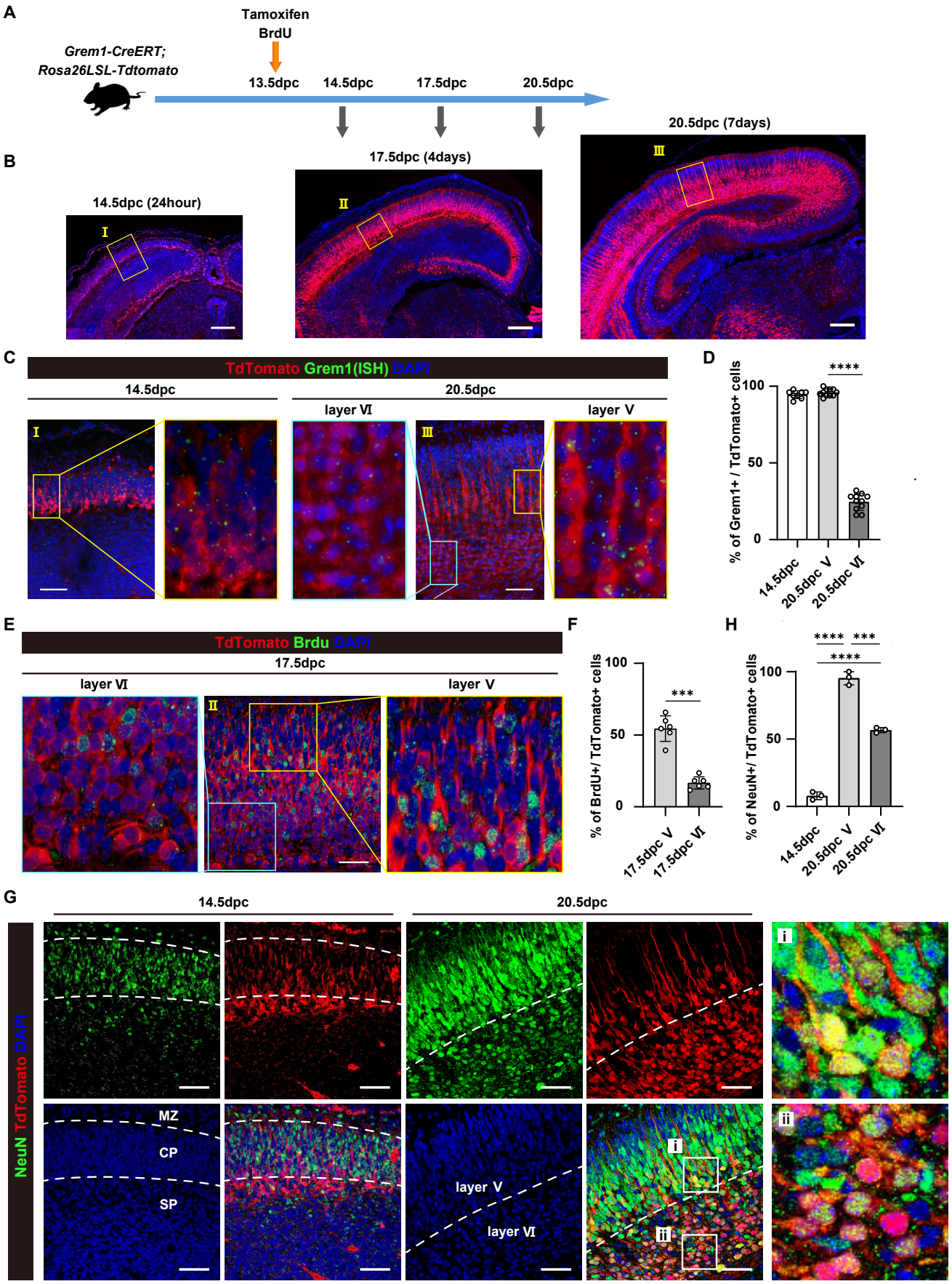
A
Tamoxifen
BrdU
Grem1-CreERT;
Rosa26LSL-Tdtomato
13.5dpc
14.5dpc
17.5dpc
20.5dpc
B
14.5dpc (24hour)
17.5dpc (4days)
20.5dpc (7days)
C
TdTomato Grem1(ISH) DAPI
14.5dpc
20.5dpc
layer VI
layer V
D
% of Grem1+ / TdTomato+ cells
****
14.5dpc
20.5dpc V
20.5dpc VI
E
TdTomato Brdu DAPI
17.5dpc
layer VI
layer V
F
% of BrdU+/ TdTomato+ cells
***
17.5dpc V
17.5dpc VI
H
% of NeuN+/ TdTomato+ cells
****
***
14.5dpc
20.5dpc V
20.5dpc VI
G
14.5dpc
20.5dpc
NeuN TdTomato DAPI
MZ
CP
SP
layer V
layer VI

Ichinose_Fig2

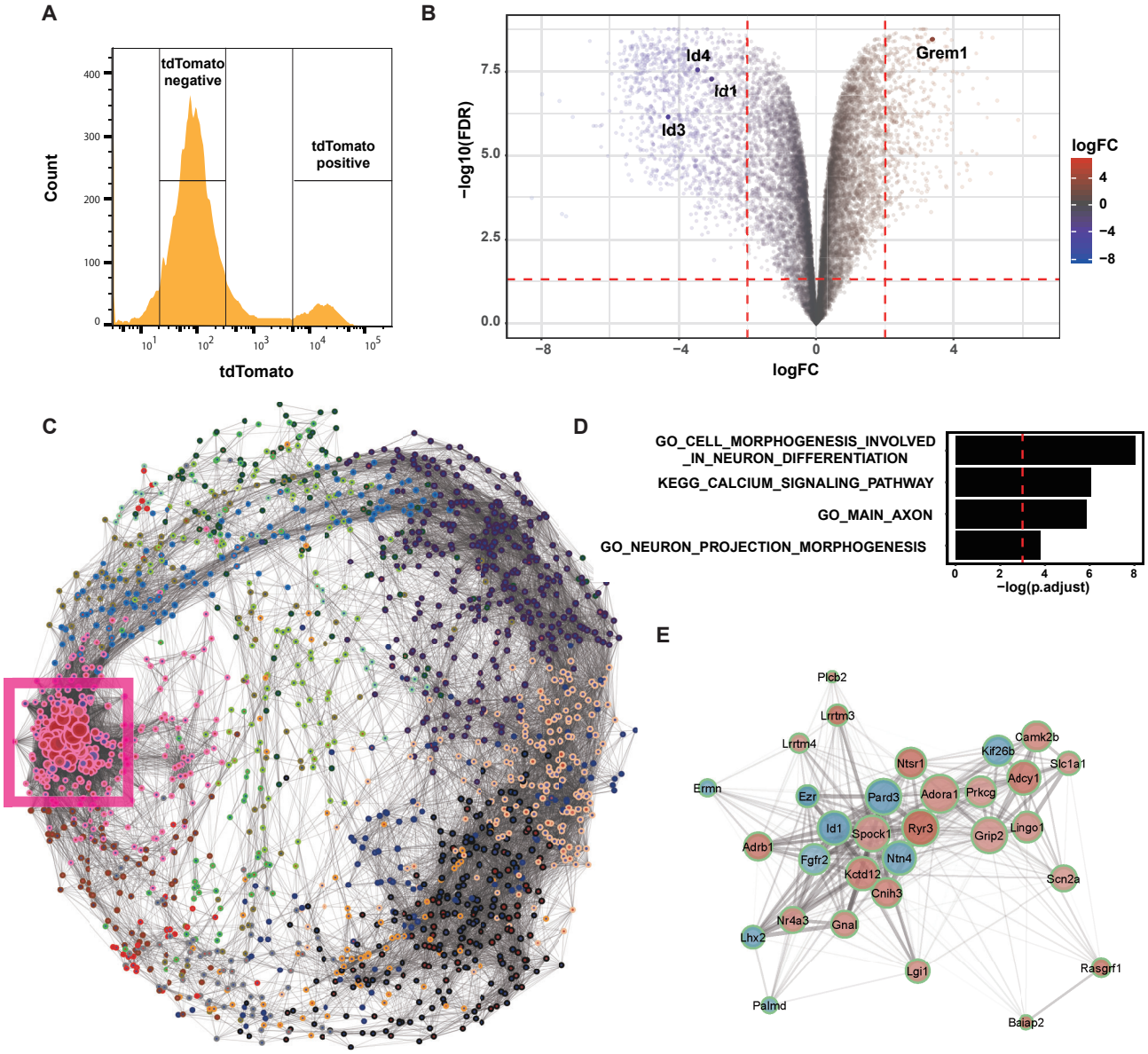

Ichinose_Fig3

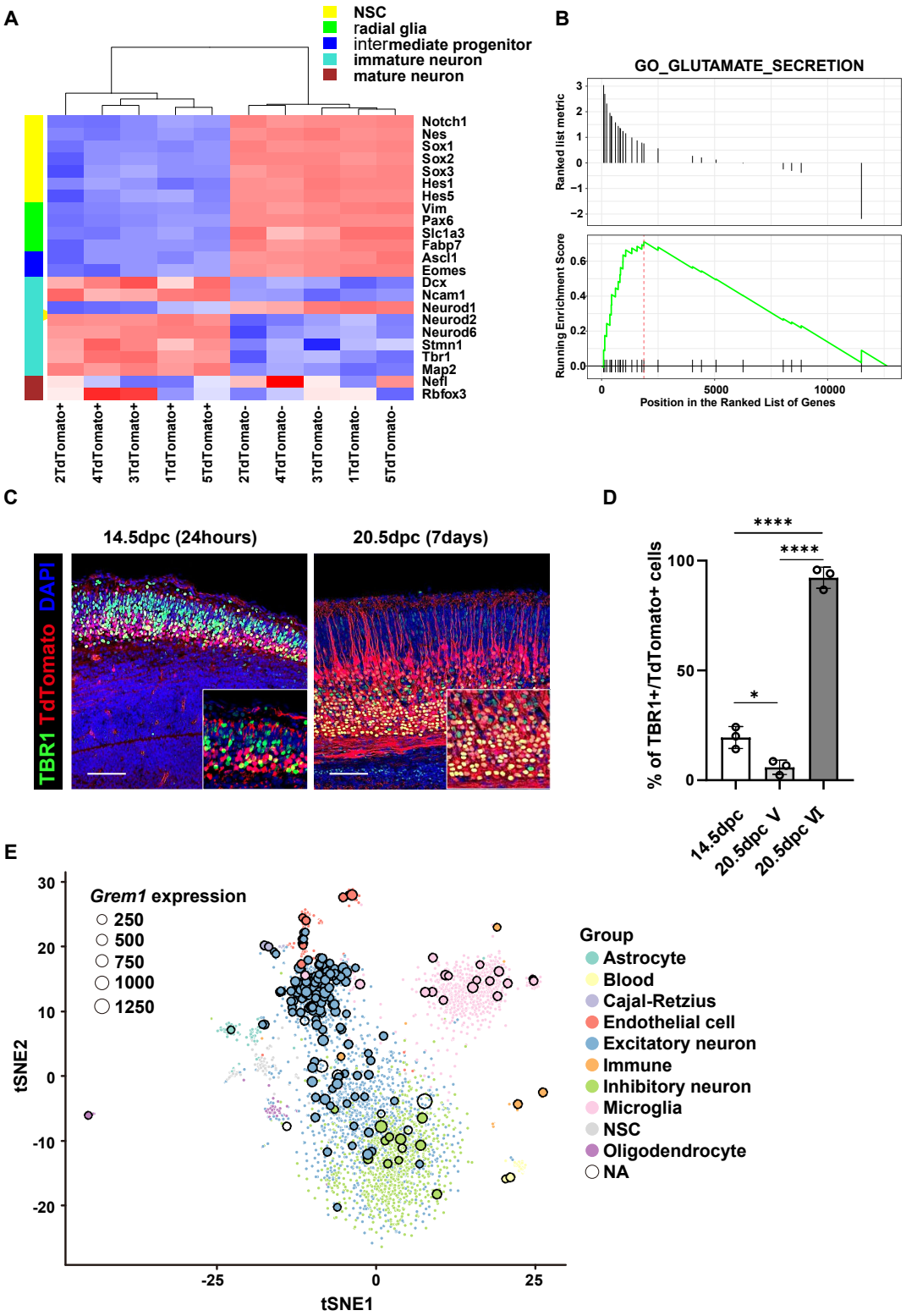

Ichinose_Fig4

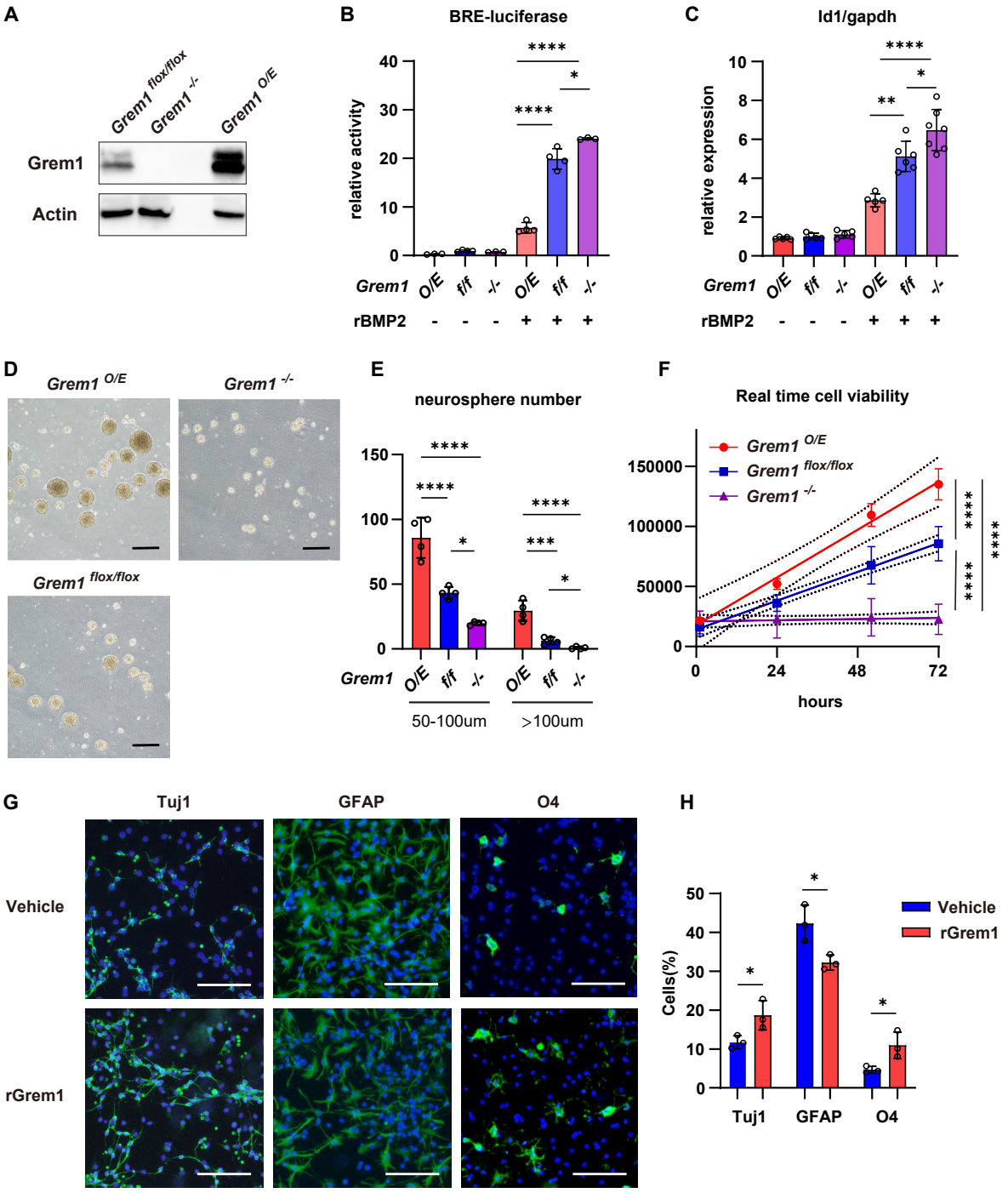

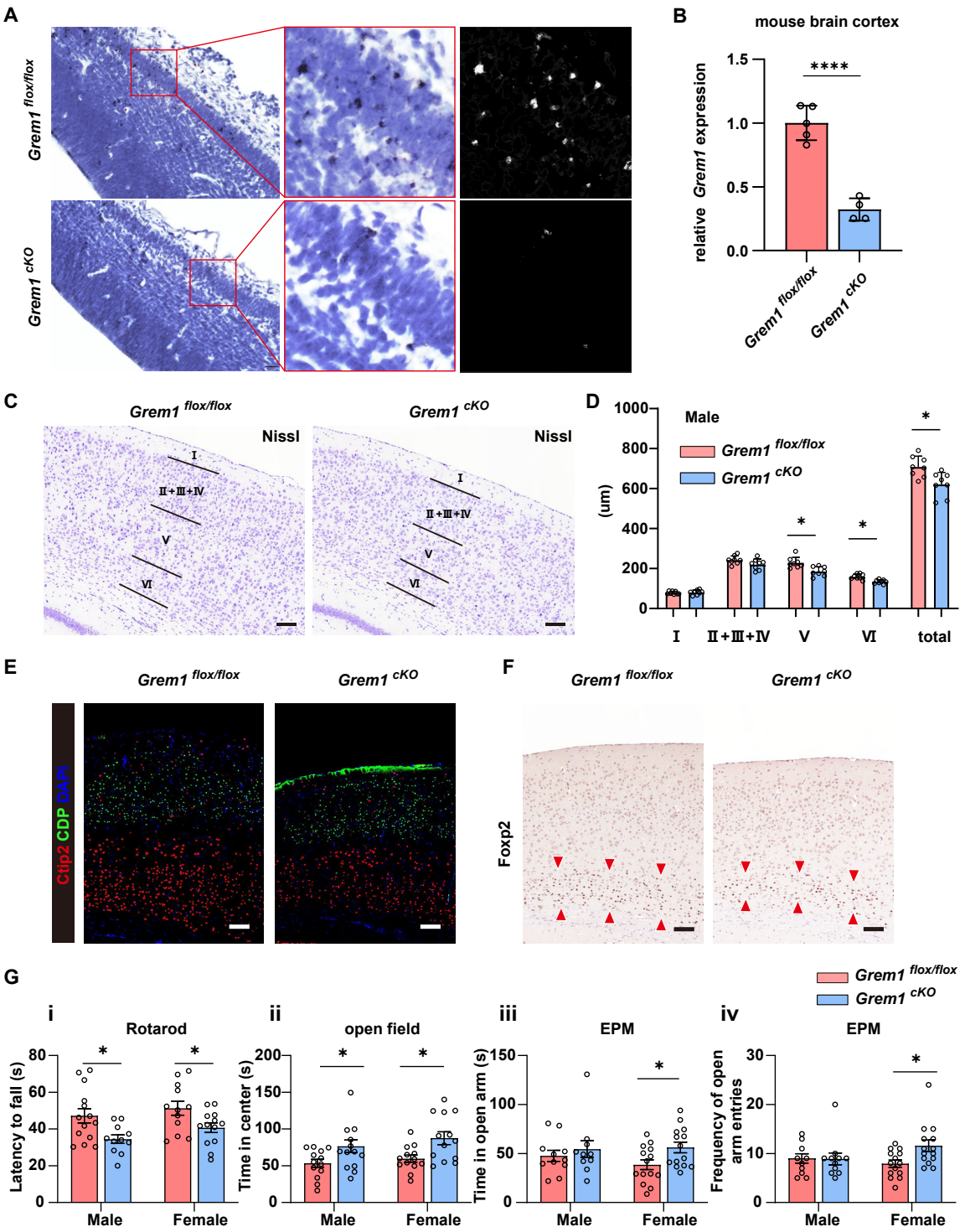
A
Grem1 flox/flox
Grem1 cKO
B
mouse brain cortex
relative Grem1 expression
1.5
1.0
0.5
0.0
****
Grem1 flox/flox
Grem1 cKO
C
Grem1 flox/flox
Grem1 cKO
Nissl
Nissl
I
II+III+IV
V
VI
D
Male
Grem1 flox/flox
Grem1 cKO
(um)
1000
800
600
400
200
0
*
*
*
I
II+III+IV
V
VI
total
E
Grem1 flox/flox
Grem1 cKO
Ctip2 CDP DAPI
F
Grem1 flox/flox
Grem1 cKO
Foxp2
G
Grem1 flox/flox
Grem1 cKO
i
Rotarod
Latency to fall (s)
80
60
40
20
0
Male
Female
ii
open field
Time in center (s)
200
150
100
50
0
Male
Female
iii
EPM
Time in open arm (s)
150
100
50
0
Male
Female
iv
EPM
Frequency of open arm entries
30
20
10
0
Male
Female